UNIVERSIDADE DE LISBOA
FACULDADE DE CIÊNCIAS
DEPARTAMENTO DE FÍSICA

Multimodal MRI analysis of the whole brain connectome of apathy in cerebral small vessel disease

João Pedro Fernandes Peixoto

Mestrado Integrado em Engenharia Biomédica e Biofísica
Perfil em Engenharia Clínica e Instrumentação Médica

Dissertação orientada por:
Ph.D. Michele Veldsman
Professor Alexandre Andrade

2019

Acknowledgements

The end is the best place to begin. As I turn the last pages of this huge chapter of my life, some people whom I deserve gratitude cross my mind.

Firstly I must acknowledge Michele for all her patience and guidance throughout this year. With her I learnt a lot. Moreover, would like to show my appreciation to the cognitive neurology lab, especially to Professor Masud Husain and all friends I've made in there, for the confidence trusted upon me and for establishing such a brilliant work environment.

I must also acknowledge Professor Alexandre Andrade for his excellent support and tutelage across the years.

Thanks mom and dad, for ensuring my survival abroad, both financially and emotionally - you're the best.

Thank you to all my friends, close or far, that always supported my endeavours and made my days so much better. All dinners, beers, cycles, climbs, talks and silences are the best memories.

Finally, I would like to show my appreciation to the support of the Erasmus+ program of the European Union for my internship abroad.

The end is the best place to begin.

Abstract

Although human studies have identified the neural mechanisms of motivated behaviour, which part of its circuitry is actually being disrupted in disease is not yet well understood. Primarily, the literature has associated apathy with reduced white matter integrity, however, the relationship between structural and functional brain changes hasn't been studied extensively in apathy. To address this concern, we've developed a comprehensive whole-brain magnetic resonance neuroimaging pipeline with which we've analysed two populations of cerebral small vessel disease (CADASIL, $n = 19$; sporadic SVD, $n = 104$). We've looked at the association between apathy and reduced white matter integrity, making use of *tract-based spatial statistics*; reduced grey matter volume with *voxel-based morphometry*; and reduced functional connectivity with a novel dynamic approach (*Leading Eigenvector Dynamic Analysis*). Furthermore, this project then aims at tying the neuroimaging findings with the parameter estimates of reward and effort sensitivity extracted through computational modelling of an effort-based decision-making task. Our results show that apathy is associated with reduced white matter integrity (reduced fractional anisotropy) of specific regions (particularly the corpus callosum and the anterior cingulum). Reduced grey matter volume of the occipital lobe seems to be associated with apathy, despite not being shown by any literature. Moreover, our results indicate that apathetic patients are associated with a weaker and more incoherent repertoire of functional connectivity than their non-apathetic counterparts. Functional connectivity associated with vmPFC regions and the occipital lobe is reduced in apathy. This shows a strong association between structural and functional changes in the brain. Apathetic patients seem to be characterised by a reduction in reward and effort sensitivity, which is associated with impaired functional connectivity. This study is a unique contributor to the understanding of the neural underpinnings of apathy in cerebral small vessel disease due to the uncommon combination of MRI modalities and relation between consequent structural and functional metrics. However, a lot more has to be done to fully understand the mechanisms of this syndrome and to extract clinically useful markers and therapies.

Keywords: Cerebral small vessel disease, CADASIL, apathy, whole-brain MRI, structural connectivity, functional connectivity.

Resumo

A revolução dos cuidados médicos do século XX e XXI possibilitou, nas últimas décadas, um crescimento sem precedente na esperança média de vida da população global. Porém, independentemente destes avanços na área da saúde, problemas associados ao declínio da função cognitiva permanecem um problema sem solução à vista. Este declínio é comummente associado ao envelhecimento. No entanto, problemas de função cognitiva são consequência de uma miríade de condições que afetam a população ao longo de todas as faixas etárias, com sintomas distintos, com grande variabilidade entre sujeitos. Demência é um termo com uma definição ampla, sendo que é caracterizada pela combinação de sintomas associados ao declínio de função cognitiva, cuja severidade conduz a uma redução de qualidade de vida. Por este motivo, a patofisiologia que conduz a demência é vasta, sendo que a sua progressão está associada a diversos fatores e condições. A segunda causa mais comum de demência é demência vascular, constituindo 15% dos casos diagnosticados (ficando apenas atrás da doença de Alzheimer). Este tipo de demência é definido pela sua associação a uma redução de fluxo nos vasos sanguíneos do cérebro. O maior contribuidor ao desenvolvimento de demência vascular é doença dos pequenos vasos cerebrais. É uma condição caracterizada pela ocorrência de enfartes lacunares, lacunas, espaços periventriculares, microhemorrogias e lesões da matéria branca. Esta condição pode estar associada ao envelhecimento e problemas de hipertensão (forma esporádica) ou pode resultar de uma mutação genética do gene NOTCH3 (forma genética, ou CADASIL). Ambas se demonstram de formas muito semelhantes, sendo que uma idade mais baixa nos pacientes hereditários esta associado a uma patologia mais limpa (com menos prevalência de outras condições) e por isso é encarado como um modelo puro desta doença. Um dos sintomas mais comuns e mais debilitantes da doença dos pequenos vasos cerebrais é apatia. Esta síndrome é definida como uma redução de motivação no comportamento do individuo (quando comparado com o seu passado) e está fortemente associada com a redução de qualidade de vida. Estudos em animais e em humanos saudáveis possibilitaram a compreensão aproximada de quais os mecanismos neurais associados com o comportamento motivado. Estes foram amplamente estudados e é aceite que possa ser caracterizado por três sistemas individuais: o primeiro sistema determina o valor subjetivo do ambiente em termos dos potenciais ganhos hedónicos e custos (sistema que envolve a parte ventral do corpo estriado e o córtex prefrontal médio); em segundo lugar, um sistema dopaminérgico (com origem na área tegmental ventral do cérebro) atua como mediador para um último sistema que age sobre o ambiente em busca de recompensas positivas (parte dorsal do corpo estriado e a parte média do giro do cíngulo). Embora este mecanismo seja conhecido, não é consensual quais as partes do sistema interrompidas ou danificadas que causam problemas neste comportamento motivado. Sendo uma condição mal estudada, a apatia em doença dos pequenos vasos abre a possibilidade a várias questões – quais as alterações estruturais associadas a apatia? Quais as alterações funcionais? Qual a relação entre as alterações? Poderá o comportamento apático servir como um bom marcador de progressão de demência vascular? Neste sentido, com o objetivo de estudar as alterações e relações entre a estrutura e função do cérebro na presença de apatia, foi criada uma pipeline de analise de ressonância magnética que visa adquirir métricas sobre a integridade da

matéria branca, a degeneração de matéria cinzenta e as alterações no reportório de conectividade funcional em duas populações com diagnostico clínico de doença dos pequenos vasos. Para além dos mais, foi também estudada a relação entre as alterações cerebrais e parâmetros de sensibilidade a recompensa e esforço obtidos através da modelação computacional de uma experiência comportamental. No âmbito deste estudo, foram recrutados 19 pacientes com CADASIL (forma hereditária de doença dos pequenos vasos cerebrais). Deste grupo, devido a incapacidade de completar a visita de ressonância, 2 participantes foram excluídos, sendo que 17 pacientes foram incluídos em todo o estudo. Foram também recrutados 104 pacientes com a forma esporádica de doença dos pequenos vasos cerebrais (associada ao envelhecimento e hipertensão). Deste segundo grupo, devido a ruído excessivo na aquisição de imagem ou complicações com o scan aquando a altura da visita, foram apenas incluídos 65 pacientes. A experiência comportamental foi completada por todos os pacientes e requeria que o doente realizasse decisões sequenciais sobre aceitar ou não uma certa recompensa (representada pelo número de maçãs numa árvore desenhada – sendo que cada maçã se traduzia num valor monetário de 1p) em troca de exercer uma certa quantidade de esforço – exercer certo nível de pressão num dinamómetro de mão, até a um máximo de 80% da capacidade máxima voluntária de cada sujeito. Os graus de recompensa e de esforço foram parametricamente controlados, igualmente distribuídos num espaço de 36 condições (6 níveis de recompensa x 6 níveis de esforço) e pseudo-aleatoriamente apresentados aos participantes. Todos os participantes realizaram um bloco de decisões, onde exploraram todo o espaço de condições para treino. Os dados de ressonância magnética foram adquiridos no mesmo scanner, recorrendo ao mesmo protocolo, para que não houvesse qualquer diferença entre os dados de cada participante. Primeiramente, os dados adquiridos foram pré-processados de forma a eliminar a maior quantidade de ruído possível. A primeira análise realizada consistia em comparar a integridade das fibras de matéria branca através dos parâmetros de difusão do fluido que neles se encontra. Mais especificamente, foi utilizada *TBSS (tract-based spatial statistics)*, uma ferramenta integrada no pacote de software FSL, para comparar os valores de anisotropia de difusão das fibras. Seria esperado observar uma redução de anisotropia no grupo de pacientes com apatia face a sua contraparte não apática. Em segundo lugar, os volumes de matéria cinzenta foram comparados, não só com o objetivo de verificar uma redução entre o grupo apático e o grupo não apático, mas também de averiguar se as regiões afetadas por esta redução coincidiam com as regiões de redução de anisotropia das fibras de matéria branca. Esta análise estrutural realizou-se utilizando *VBM (voxel-based morphometry)*. Em último lugar avaliou-se a conectividade funcional. Esta foi aferida de duas abordagens distintas: em primeiro lugar, utilizou-se uma metodologia que não considera a existência de flutuações de conectividade funcional ao longo da aquisição dos dados (dual regression) e uma que tinha por base a relevância da sua flutuação ao longo da aquisição para a compreensão da conectividade funcional (*Leading Eigenvector Dynamics Analysis*). Todos os modelos estatísticos aplicados foram controlados com covariáveis sem interesse (idade, género e dano causado na matéria branca) e corrigidas para erros de comparações múltiplas.

Os nossos resultados fornecem provas de associação entre apatia e redução de integridade da

matéria branca em certas regiões (especificamente no corpo caloso e no cíngulo anterior). Por outro lado, mostram também que o comportamento apático está associado a uma redução de volume da matéria cinzenta em regiões do lobo occipital na população de CADASIL, sendo que o mesmo não foi observado na versão esporádica. É interessante constatar que os nossos resultados parecem indicar uma associação entre a integridade da matéria branca e a degeneração da matéria cinzenta. Além do mais, os resultados demonstram enfraquecimento da conectividade funcional. Estas alterações funcionais parecem ser parcialmente derivadas das alterações estruturais, porém, não são totalmente moduladas por estas. Estes resultados não só fortalecem o argumento de que o conectoma funcional não é inteiramente definido pela anatomia cerebral, mas também que métricas de conectividade funcional podem ser marcadores úteis de diagnóstico de doença e podem conduzir a novas aplicações para tratamento de apatia. Embora as suas limitações sejam evidentes (como por exemplo o número reduzido de sujeitos por grupo, resolução do protocolo de imagem) e bastantes ideias tenham ficado por explorar (por exemplo, o impacto da severidade da condição nos conectomas), este estudo é um primeiro exemplo da utilidade da informação obtida aquando do estudo dos conectomas estruturais e funcionais em simultâneo. É também pioneiro na apresentação do conceito de uma rede funcional ligada a um comportamento motivado.

Keywords: Doença dos pequenos vasos cerebrais, CADASIL, apatia, whole-brain MRI, conectividade estrutural, conectividade funcional.

Contents

List of Figures

List of Tables

List of Abbreviations

BOLD	**B**lood **O**xygenation **L**evel **D**ependent
CADASIL	**C**erebral **A**utosomal **D**ominant **A**rteriopathy w/ **S**ubcortical **I**nfarcts and **L**leukoencephalopa
FA	**F**ractional **A**nisotropy
LEiDA	**L**eading **Ei**genvector **D**ynamics **A**nalysis
MELODIC	**M**ultivariate **E**xploratory **L**inear **D**ecomposition into **I**ndependent **C**omponents
MRI	**M**agnetic **R**esonance **I**maging
TBSS	**T**ract-**B**ased **S**patial **S**tatistics
SVD	**S**mall **V**essel **D**isease
VBM	**V**oxel-**B**ased **M**orphometry
WMH	**W**hite **M**atter **H**yperintensity

1 Introduction

1.1 Cognitive impairment, vascular dementia and cerebral small vessel disease

Paradigm-shifting advances in the medical sciences seen in the last decades have allowed an unprecedented improvement in the general population's quality of life. However, despite the increased quality of mainstream healthcare and lifestyle practices, decline of brain function is still an issue with an elusive solution. Although it's usually associated with life's later stages, cognitive impairment can be brought about through a myriad of neurological disorders, which affect populations across all age groups. As such, these neurological disorders have been of growing concern of the XXI century healthcare.
Dementia is a broad concept, which describes a set of symptoms associated with an ongoing decline in brain function (including, among others, memory loss, difficulties in thinking, motivated behaviour, problem-solving or language) and which impair the patient's quality of life. The pathophysiology of dementia is quite diverse [1], and a myriad of conditions contribute to its progression. Moreover, these conditions often happen simultaneously, with big inter-subject variability and with different patterns from one disorder to the other. As such, the origins of dementia have been widely studied in order to understand their mechanisms, with the hopes of generating treatment alternatives for such conditions. Vascular dementia is no exception and, as such, its roots aren't yet totally understood; however, a major feature of this condition is the reduced blood flow to the brain driven by pathology of the vessels. Studies of vascular dementia show it is the second most common cause of dementia after Alzheimer's disease (Figure 1.1) [2], making up around 15% of diagnosed dementia cases, estimating to affect 150.000 individuals just in the UK alone [3].

Vascular dementia shows a broad spectrum of cognitive changes which vary based on which neural circuitry is affected by the different vascular pathologies (Table 1.1). Due to damage being frequently present in the areas of the frontal striatum, deficits in attention, information processing and motivation are often seen [5], [6].

However, the major contributor to the occurrence of vascular dementia is cerebral small vessel disease (cerebral SVD). This refers to a group of pathological processes with various origins that affect the small arteries, arterioles, venules and capillaries of the brain. There are different types of cerebral SVD and a simplified classification can separate it into a sporadic (related to

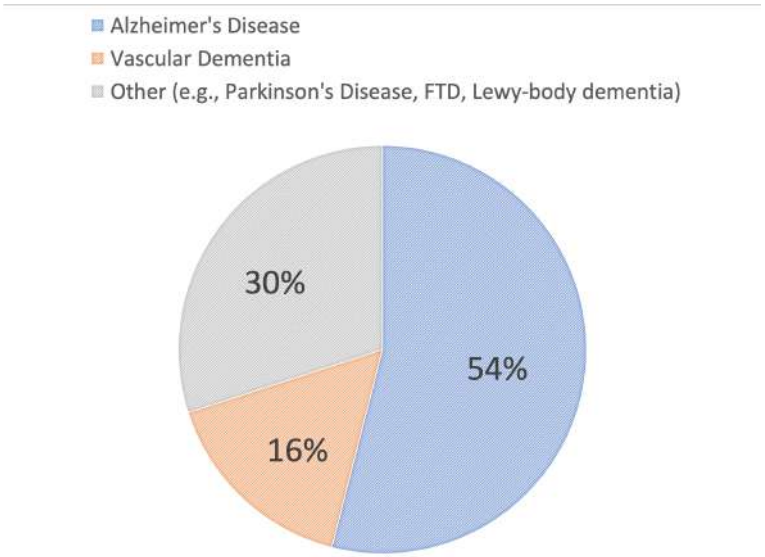

FIGURE 1.1: Prevalence of different types of dementia in the general population [4].

TABLE 1.1: Subtypes of vascular disease contributing to vascular dementia. Adapted from **OBrien2015**

Imaging and pathological changes in vascular dementia	
Cortical vascular disease	Multiple cortical infarcts
Small vessel disease	Lacunes, extensive white matter lesions, infarcts, demyelination
Strategic infarct disease	Infarct in strategic location (e.g. thalamus)
Hypoperfusion disease	Watershed infarcts, white matter lesions
Genetic small vessel disease (CADASIL)	Multiple lacunes, white matter lesions, temporal lobe white matter affected
Alzheimer's disease with cardiovascular disease	Combination of vascular changes and atrophy, especially medial temporal lobe, mixture of vascular and degenerative pathology

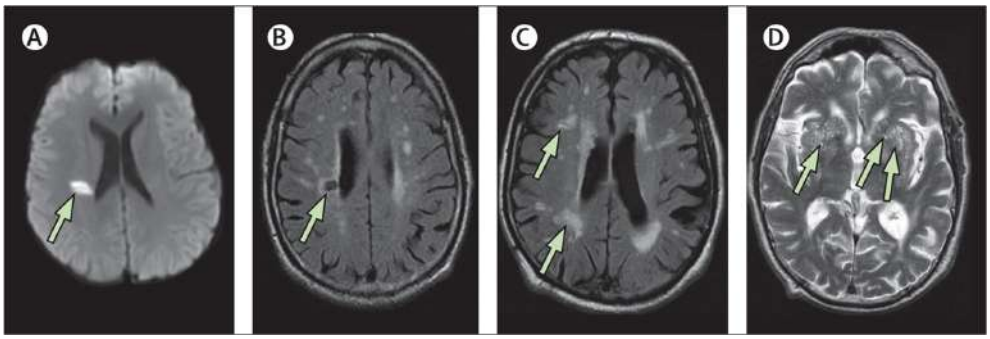

FIGURE 1.2: Key imaging characteristics of features of cerebral small vessel disease. A) lacunar infarct, B) lacune, C) white matter hyperintensities, D) microbleeds. Taken from [16].

aging and hypertension) SVD and a genetic form of SVD (e.g. CADASIL - cerebral autosomal dominant arteriopathy with subcortical infarcts and leukoencephalopathy) [7].

1.2 Pathology of cerebral small vessel disease

The main imaging features of cerebral SVD include acute lacunar (or small subcortical) infarcts or haemorrhages, lacunes (fluid-filled cavities thought to show old infarcts, many clinically silent) [8], white matter hyperintensities [9], perivascular spaces [10], microbleeds [11] and brain atrophy [12]. Additional damage is detectable with diffusion tensor imaging and shows altered white matter integrity, disrupted axonal connections, and altered myelination (Figure 1.2) [13]. Cerebral small vessel disease is responsible for around 25% of all ischemic strokes, as well as a considerable amount of encephalopathy. Cerebral SVD is often tied to several domains of cognitive impairment, however a common hallmark to both the sporadic and genetic version is apathy [14], [15].

Sporadic cerebral SVD is a phenomenon that's common with aging and which risk is increased by hypertension and diabetes. White matter lesions often occur in the brain after the 65 years of age. The pathophysiology and imaging features of the genetic form of SVD – CADASIL – are very similar to those of sporadic SVD. However, on the other hand, CADASIL is prominent in a younger population. This means that CADASIL patients often lack other comorbidities due to aging seen in sporadic forms of SVD. As consequence, CADASIL can be seen as a model of pure vascular pathology. Moreover, CADASIL patients tendentially show a more variable pattern of white-matter lesions. CADASIL is a condition derived from the mutation of the NOTCH3 gene (Notch homolog 3). Mutation of this gene alter the number of cysteine residues of the NOTCH3, which accumulate in the small vessels of affected individuals.

TABLE 1.2: Prevalence of apathy as a symptom of different types of conditions. Adapted from [25]

Condition	**Prevalence**	**Comments**
Parkinson's Disease	30%	Non-motor symptom of PD. Occurs at all stages of PD. Clear evidence it is an intrinsic (rather than reactive feature of PD) [22].
Alzheimer's Disease	50%	Along with PD, apathy in AD has had the greatest level of research interest to date [23].
Sporadic small vessel disease (SVD)	15% - 30%	An increasingly recognised complication of SVD, with a clear association between apathy and both background vascular risk factors and imaging changes of SVD.
CADASIL	40%	One of the cardinal features of this condition. Occurs at all clinical stages but more likely with progression of the disease [24].
Stroke	30%	Occurrence is associated with worse outcomes and poorer quality of life.
Frontotemporal Dementia	50%	A core feature of behavioural variant FTD (which can have different underlying pathologies), although also present in other subtypes. Strongly associated with impulsivity.
Amyotrophic lateral sclerosis	40%	A common feature, with at least mild apathy symptoms present in most patients.
Depression	38%	Dissociable from, but associated with the syndrome of depression, particularly anhedonic components.

1.3 Apathy and the neural mechanisms underlying motivated behaviour

Apathy is a common syndrome that occurs across a range of neurological and psychiatric disorders (Table 1.2). It has been conceptualized as a behavioural syndrome of loss of motivation when compared to a patient's previous level of functioning [17]. It has been extensively associated with reduced quality of life [18] and thus it has been widely studied in many conditions. It has been highly studied in the domains of Alzheimer's and Parkinson's disease, however, their mechanisms in small vessel are still illusive [19]. A richer understanding of the cognitive and neural mechanisms of apathy in cerebral SVD might potentially be of importance for the development of future therapies and its use as a biomarker of developing vascular dementia.

Motivated behaviour is characterised by an active effort to pursue and obtain rewards. The literature provides insights that indicate that this behaviour is comprised of three fundamental neural processes (Figure 1.3) [20]. Firstly, an internal system determines the subjective value of events in the environment in terms of their hedonic gain as well as their potential costs

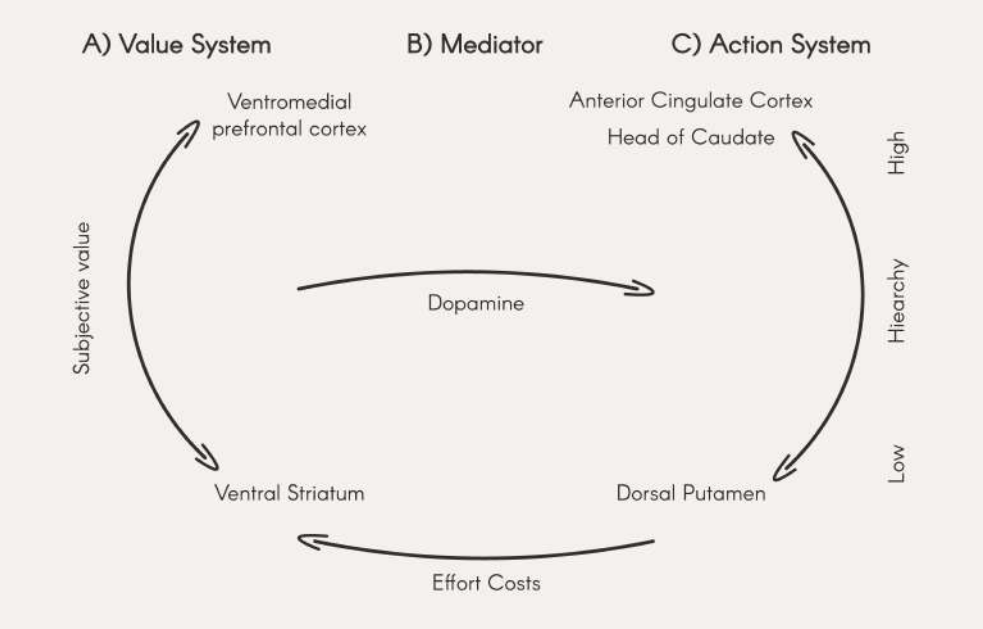

FIGURE 1.3: Conceptual framework and brain basis of motivated behaviour. A valuation system computes the subjective value of the current and potential events. A mediating system integrates this information to activate the motor system towards particular goals. A motor system produces behaviour towards motivationally relevant stimuli. These processes are instantiated within a complex network of reciprocally connected cortical and subcortical brain regions, under the influence of the mesolimbic dopaminergic system.

(e.g. physical or cognitive effort, temporal proximity). Secondly, a mediation system activates behaviour towards particular goals. Lastly, an action system must act on the environment in order to pursue positive outcomes.

Previous studies on motivated behaviour have identified that the value system includes areas such as the ventral striatum, VS, (including the nucleus accumbens, NAc, and the ventral-rostral putamen) and the ventromedial prefrontral cortex, vmPFC, (which includes the most rostral areas of the anterior cingulate cortex, ACC, and adjacent areas of the medial orbitofrontal cortex, OFC) [21]. There is evidence that the VS mediates a process of conditioning learning, in which current states of the environment predict future rewards [22]. On the other hand, the hallmark of vmPFC function is its flexibility: although activity within it is also sensitive to the subjective value of the events, there is evidence that this activity varies dynamically, as if values are being reassessed at each instant [21], [23]. This flexibility appears to support rapid shifts in preference. Once computed in the first system, the information of value must be translated into appropriate behavioural responses. The neural circuitry underlying this mediating system is complex and distributed. However, it is widely accepted, in behavioural neuroscience, that both the VS and ACC serve as crucial interfaces, under the influence of the mesolimbic dopamine system, which originates in the ventral tegmental area of the midbrain. Although dopamine is a key modulator, it is acknowledged that other neurotransmitter systems may also play a role

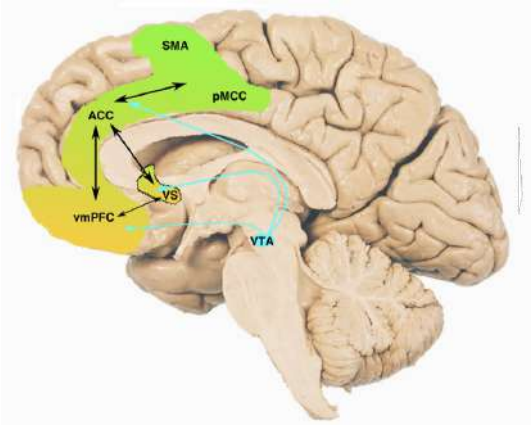

FIGURE 1.4: Diagram of the brain areas involved in the motivated behaviour pathways. Adapted from [25].

[24].

Finally, the production of behaviour is mediated by the posterior mid-cingulate cortex and dorsal striatum. Although conceptually useful for understanding the different components contributing to motivated behaviour, it is unlikely that the proposed systems exist as discrete entities within the brain.

1.4 MRI and neuroimaging findings

Understanding the neural basis of apathy may lead to novel approaches for prediction, diagnosis or treatment. For this, studying the anatomy and function of the brain and comparing it across patient populations is essential. As such, magnetic resonance imaging (MRI) can be employed. This imaging technique is a very powerful and versatile method with the ability to safely and non-invasively measure a wide range of properties of the living brain. The great flexibility of MRI arises from the myriad of ways in which it can be used to manipulate and measure signals from tissues. There is a wide variety in the modalities of images that can be acquired on an MRI scanner, which allow to capture different information about the brain. However, there are three modalities that are by far the most commonly used in neuroimaging research: structural, diffusion and functional imaging (Figure 1.5).

The first, structural imaging, provides information about gross anatomical structures in the brain (e.g. showing boundaries of the cerebral cortex). The second modality, diffusion imaging, diffusion weighted imaging or diffusion MRI (dMRI), provides information about the microstructure and anatomical connectivity within the brain (by measuring the diffusivity of fluid inside white matter tracts). The third, functional imaging, or functional MRI (fMRI), provides information about the activity of neurons in the brain by measuring fluctuations in deoxyhemoglobin concentration linked to neural activity - the so-called blood oxygenation level dependent (BOLD)

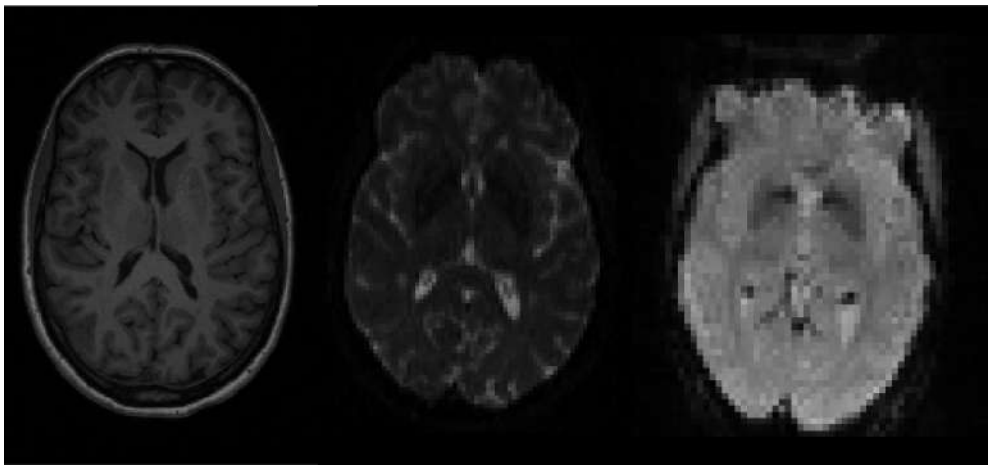

FIGURE 1.5: Examples of the three most commonly used MRI modalities. From left to right: structural T1-weighted imaging, diffusion weighted imaging and functional imaging.

effect - either in response to specific stimuli or tasks (task fMRI) or in relation to the spontaneous activity of the neurons (resting state fMRI).

1.4.1 dMRI and structural connectome

In a general perspective, the white matter is composed of several tracts that spread across the brain and that communicate with each in different networks, simultaneously serving different purposes and processes. To understand the functioning of a network, one must first get to know its elements and their relations. To that end, the development of advanced tractography algorithms applied to dMRI (which make use of the estimates of water and CSF diffusion coefficients) has allowed the detection, non-invasively, at the whole-brain level or of specific regions, of white matter fibre tracts connecting brain areas [26], [27]. This knowledge allowed for the construction of large-scale networks reflecting the anatomical connectivity of the brain. Furthermore, it provided mechanistic insights into how the brain function is affected by the disruption of its structure. The structural connectome is most often represented as a combination of anatomically distinct brain regions and the neural pathways that link them. Despite the lack of a single universally accepted parcellation scheme, this is the most feasible organisational level for the human connectome. Considering this macro-scale of brain parcellations, the structural connectome of healthy adults remains relatively stable when compared to the rapid changes occurring at the functional level. Structural alterations occurring at this macro-scale, either associated with the brain's natural development of ageing or in disease, are typically slow [28]. Drastic changes in this connectome are usually associated with disease. Note, however, that the entire map of neural connections ambitioned by the Human Connectome Project (www.humanconnectomeproject.org) may reveal higher individual variability and changes over shorter time-scales.

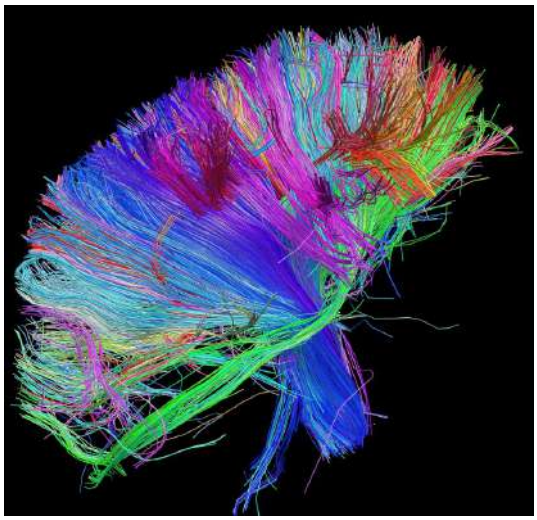

FIGURE 1.6: White matter fiber architecture of the brain. Measured from diffusion spectral imaging (DSI). The fibers are color-coded by direction: red = left-right, green = anterior-posterior, blue = through brain stem. Taken from humanconnectomeproject.org.

1.4.2 Resting state fMRI and functional connectivity

Resting state fMRI uses the same type of MRI acquisition as task fMRI, the only difference being that the participant is not asked to perform any specific task. Then, the signal in these resting state scans reflects spontaneous brain activity; and it is the coactivation between different locations that provides a measure of functional connectivity. In the last two decades, since the seminal discovery of synchronous brain activity despite the absence of a task or stimulus, resting-state fMRI has shed new light on the spatiotemporal organisation of spontaneous brain activity. Ever since, countless studies have been produced aiming at understanding the functional connectome – the map of correlations of neural activity across the brain. These, in spite of being based on the structural connectome, seem to transcend it, as it has been shown that different brain areas, not structurally connected, show functional coactivation [29]. In the beginning, it was considered that the functional connectome did not significantly change over time (as it was with the structural connectome) and thus, its analysis was done in a static perspective (taking an average of the signal over the acquisition time). However, recent neuroimaging studies have shown that meaningful large-scale functional networks fluctuate over time, from correlations with the BOLD signal, implying that measures assuming stationarity of over a full resting-state acquisition may be too simplistic to capture the full extent of brain activity [30]. Furthermore, interestingly, the expanding idea is that functional connectivity evolves as a multi-stable process, passing through multiple and reoccurring discrete functional states, rather than varying in a more continuous sense. These initial findings have raised several questions about the nature of brain dynamics and their implications on behaviour and disease and thus, a body of research has rapidly blossomed to investigate the now coined functional connectivity dynamics.

1.4.3 Neuroimaging findings of apathy in cerebral SVD

Two whole brain diffusion studies, one with 121 and the other with 331 sporadic SVD patients have shown apathy is associated with reduced integrity of white matter tracts of cingulate and thalamic regions. In contrast, no significant results were obtained when depression was used as a regressor of interest [32], [33]. Moreover, a recent study, combining behavioural and diffusion imaging paradigms has investigated apathy in the genetic form of SVD – CADASIL. This study, using a seed-based tract-based spatial statistics analysis provided evidence that linked impairment of motivated behavioural to a decrease in integrity of white tracks in regions of importance to the motivated-behaviour system (e.g. left anterior cingulum, bilateral orbitofrontal-anterior cingulate white matter tracts) [20]. Together, these studies seem to provide sufficient evidence of the link between reduced white matter integrity in specific regions and apathy in cerebral SVD (sporadic and genetic). In CADASIL, a study looked at cortex morphology and how it changed with apathy. Such study shows that the morphology of the mediofrontal and orbitofrontal cortices are altered in apathetic patients, (reduction of sulcal depth), however no modifications of the cortical thickness are shown. These results orientate toward underlying mechanisms distinct from the reduction of cortical thickness and suggest that other processes are involved in these cortical morphologic alterations, such as reduction of cortical surface due to disappearance of intracortical columns [34]. However, literature indicates that cortical surface, cortical thickness and grey matter volume change at different rates and with age and disease [35], [36]. It also seems to provide evidence that different cortical measures have different sensitivity to pathology [37], [38].

Functional connectivity has been demonstrated to be disturbed in CADASIL patients and related to cognitive impairment when compared to healthy controls [39]. Moreover, disrupted functional connectivity has been shown to be driven by apathy in certain pathologies [40], [41]. However, to the best of our knowledge, the mechanisms of functional connectivity and the implications grey and white matter changes have on it have not been studied in apathy related to cerebral SVD.

1.5 Overview of the Thesis

This dissertation reflects the work of a 9-month project comprised of an internship at the Cognitive Neurology Centre (CNC) of the University of Oxford, in the United Kingdom, led by Professor Masud Husain, under the supervision of PhD Michele Veldsman and in collaboration with the Hedonia: Translational Research Group, led by Professor Morten Kringelbach. //

Based on previous literature about the neural mechanisms of apathy, cerebral small vessel disease, and brain changes with pathology, this study aims at studying the changes identified in

the brain through different MR imaging modalities and the relation between functional connectivity and computational modelling parameters of an effort-based decision-making task in two cerebral SVD cohorts (19 CADASIL and 104 sporadic SVD patients).

Based on previous literature and our understanding of the pathology of these patients, we expect that:

- Grey matter volume is reduced in apathy in cerebral SVD;
- Functional connectivity is weaker in apathy;
- Functional connectivity strength is positively associated with grey matter volume;
- The association between functional connectivity and grey matter volume is reduced when covaried for white matter integrity;
- Functional connectivity changes in apathy are associated with reduced reward and effort sensitivity.

With this project we aim at better understanding the neural subtracts of apathy in cerebral SVD. It's the first step, without making use of longitudinal data, to probe the hypothesis of apathy possibly being a marker of vascular dementia in the cerebral SVD populations. Preliminary results were presented at the *9th International Symposium on Biology of Decision Making* and the *4th UK Dementia MRI Conference*.

2 Methods

2.1 Ethics

This study was approved by the ethics committee of the University of Oxford and written informed consent was obtained from all participants, in accordance with the Declaration of Helsinki.

2.2 Demographics

Nineteen patients with CADASIL were enrolled from two regional neurological centres (Oxford and Cambridge, UK). In order to qualify for the study, all patients had a confirmed clinical diagnosis of CADASIL (cysteine changing NOTCH3 mutations). Their ages ranged from 33 to 70 (mean = 54.3±10.5), 13 of them females. Exclusion criteria included physical disability to the extent of one being unable to squeeze a handheld dynamometer, previously documented large vessel stroke and MRI incompatibility. Seventeen of the enrolled patients completed cognitive questionnaires, behavioural testing and MR imaging acquisition. However, two patients were excluded from the imaging acquisition (one due to extreme claustrophobia and the other due the occurrence of an acute clinical event between the behavioural and imaging visits). More detailed information about the demographics of this cohort can be found in Table 2.1.

One hundred and four patients with sporadic SVD were enrolled from a neurological centre in Oxford, UK. All patients had a confirmed clinical diagnosis of sporadic small vessel disease. The same exclusion criteria from above was applied. All patients complete cognitive and behavioural testing as well MR imaging acquisition. However, from the initial cohort, sixty-five were selected to enroll this study, either due to scanner malfunction in some cases, and excessive noise found in the scans for others. More detailed information about the demographics of this cohort can be found in Table 2.2.

Table 2.1: CADASIL group demographics.

Measure	**CADASIL (n=18)**	**No apathy (n=8)**	**Apathy (n=10)**
Age	54.3 ± 10.5	55.7 ± 11.1	52.6 ± 10.4
Sex (f/m)	12/6	6/2	6/4

Table 2.2: Sporadic SVD group demographics.

Measure	Sporadic SVD (n=104)	No apathy (n=59)	Apathy (n=45)
Age	67.3 ± 11.8	67.2 ± 12.2	67.4 ± 11.4
Sex (f/m)	45/59	28/31	17/28

2.3 Disease and cognitive measures

Apathy was assessed making use of the Apathy Evaluation Scale (AES) [42] as well as the Lille Apathy Rating Scale (LARS) [43]. An individual was defined as apathetic if either the LARS score was above -22 or the AES score was above 37 (equivalent to at least mild-moderate apathy). Depression was measured using the Beck Depression Inventory (BDI) [44] and the Geriatric Depression Scale (GDS) [45]. Baseline cognitive levels were formally assessed using the Addenbrooke's cognitive examination III (ACE-III) [46]. Quality of life was assessed using a Cantril Ladder, in which participants rated their overall current quality of life on a visual scale ranging from 1-10, and the Well-Being Index (WHO-5) [47].

2.4 Effort-based decision-making behavioural experimental design

Participants were asked to complete an effort-based decision-making task on a computer running Psychtoolbox (psychotoolbox.org) implemented within MATLAB (MathWorks). The task required the patient to make decisions of whether to accept an offer of a certain amount of reward in return for exerting a certain amount of effort via an individually calibrated handheld dynamometers (SS25LA, BIOPAC Systems). Each offer was presented on the screen as an apple tree with a certain number of apples. Reward for each trial was indicated by the number of apples on the cartoon tree (1, 3, 6, 9, 12 or 15) and numerically displayed underneath it. Each apple was worth 1p. Effort required to obtain the reward was indicated by the height of a yellow bar on the cartoon tree trunk, with the six possible levels (corresponding to 10, 24, 38, 52, 66 and 80% of a participant's maximal voluntary contraction).

The six reward and six effort levels were combined, and the resultant 36 conditions (Figure 2.2)were sampled evenly in a pseudo-randomized order (meaning that all participants received the same offers, presented in the same order) across five blocks, for a total of 180 trials.

Participants were instructed to weigh up the effort costs against the reward on offer for each trial and decide if it's worth squeezing that hard for that number of apples (in which a higher number of apples translated into a larger sum of monetary value – 1 apple = 1p). If they accepted an offer (by exerting a small squeeze on the left handgrip) they had to squeeze to the required force and hold above this level for at least 1s within a 5s response window, after which they

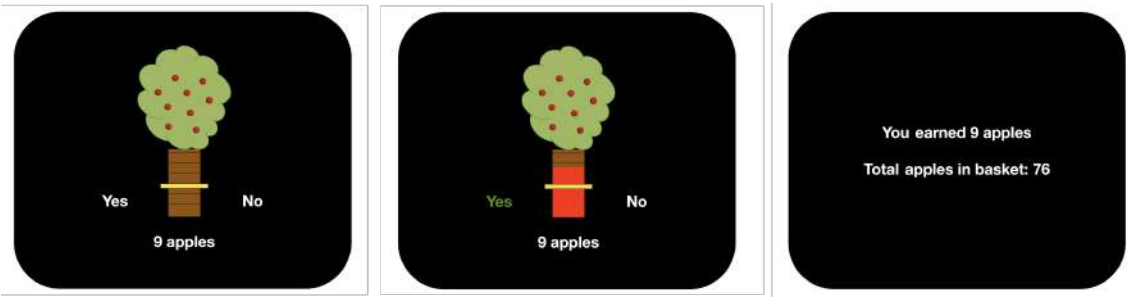

FIGURE 2.1: On a trial by trial basis participants were presented with offers (apples on a tree, with each worth 1p) in return for exerting physical effort (ranging from 10% to 80% of a subject's previously determined maximal voluntary contraction (MVC). If they accepted the offer (by squeezing the left-hand grip) the tree moved to the left or right of the screen, indicating which hand they had to respond with. They had a 5-s window within which to achieve the required force level. If they rejected the offer (by squeezing the right-hand grip) they waited the same 5-s period.

FIGURE 2.2: The 6 x 6 decision space in which participants worked through 180 trials, pseudo-randomly, evenly sampled over five blocks.

were granted with the apples on offer. During the squeeze, live feedback of the force executed was shown as a red bar that indicated current force relative to the target line. Conversely, if participants rejected an offer (by exerting a small squeeze on the right handgrip) they waited an equivalent time (to control for temporal discounting effects) before moving onto the next offer. Therefore, on each trial participants decided whether the value of an offer was worth engaging with, compared to doing nothing for the equivalent time. Before starting the experiment, the handles were calibrated to account for the strength of each individuals. Participants were also given trials to practice each force level with each hand to familiarise themselves with the effort required. Lastly, they completed a practice block in which they made decisions on the full range of options in the experiment.

2.5 Neuroimaging data acquisition

All patients enrolled in this study (either genetic or sporadic SVD) were scanned at the Acute Vascular Imaging Centre (AVIC) of the John Radcliffe Hospital, Oxford, with the same equipment and protocol. The site makes use of a 3T Siemens Magnetom Verio syngo with a 12-channel head coil. The full protocol used comprised 13 different sequences, lasting for around 50 minutes. To make the envisioned imaging analysis possible, five sequences from three different modalities were used for this study. To obtain high resolution images of the anatomy of the brain and the white matter damage, two structural sequences - a T1-weighted and a T2-FLAIR (fluid-attenuated inversion recovery) sequence - were acquired.

For white matter integrity analysis and the correction of susceptibility distortions, a dMRI sequence was acquired. For the above described sequences, the patients were just instructed to lay in the scanner as still as possible.

Finally, for the functional connectivity analysis, a resting state fMRI sequence was acquired. For this sequence, dummy volumes were automatically discarded by the scanner to account for T1 stabilization. Participants were instructed to lay as still as possible, with their eyes open, focused on a fixation cross on top of the scanner.

No reshimming took place between each sequence and the full protocol was run in the same order in just one go for all participants. This allowed for the construction of field maps.

2.6 Neuroimaging data analysis

All steps, from preprocessing to actual analysis, were implemented using bash (v3.2.57), FMRIB Software Library (FSL v5.0.11 fsl.fmrib.ox.ac.uk/fsl), Statistical Parametric Mapping (SPM12 spm/software/spm12/) and MATLAB_R2015b (MathWorks, USA). All scripts can be found in the following GITLAB repository: https://gitlab.com/jpeixoto18/dissertation_scripts.

Table 2.3: MRI parameters of the structural sequences

Parameter	**T1-weighted**	**T2-weighted FLAIR**
Acquisition time	4:54 min	4:32 min
PAT	2 (GRAPPA)	Off
Voxel size	1.0 x 1.0 x 1.0 mm	1.0 x 1.0 x 3.0 mm
SNR	1.00	1.0
Orientation	Sagittal	Coronal
Phase encoding direction	A >>P	R >>L
Slices	208	50
FoV read	256 mm	192 mm
Slice thickness	1.0 mm	3.0 mm
TR	2000 ms	9000 ms
TE	1.94 ms	88 ms
TI	880 ms	2500 ms
Flip angle	8 degrees	150 degrees
Matrix coil mode	Triple	CP
Echo spacing	5.9 ms	12.5 ms
Multi-slice mode	Single shot	Interleaved

Table 2.4: MRI parameters of the dMRI sequences

Parameter	**Diffusion weighted**	**b-value = 0, PA encoding direction**
Acquisition time	4:40 min	0:32 min
PAT	2 (GRAPPA)	2 (GRAPPA)
Voxel size	2.0 x 2.0 x 2.0 mm	2.0 x 2.0 x 2.0 mm
SNR	1.0	1.0
Orientation	Transversal	Transversal
Phase encoding direction	A >>P	P >>A
Slices	64	64
FoV read	192 mm	192 mm
Slice thickness	2.0 mm	2.0 mm
TR	8000 ms	8000 ms
TE	86.0 ms	86 ms
Matrix coil mode	Triple	Triple
Echo spacing	0.68 ms	0.68 ms
Multi-slice mode	Interleaved	Interleaved
b-value	1500 s/mm2	0 s/mm2
Diffusion directions	32	32

TABLE 2.5: MRI parameters of the resting-state fMRI sequence.

Parameter	**Resting-state**
Acquisition time	5:35 min
PAT	Off
Voxel size	3.0 x 3.0 x 3.0 mm
SNR	1.0
Orientation	Transversal
Phase encoding direction	A >>P
Slices	46
FoV read	192 mm
Slice thickness	3.0 mm
TR	1640 ms
TE	30 ms
Multi-band acceleration factor	2
Flip angle	90 degrees
Volumes	200
Matrix coil mode	Triple
Echo spacing	0.7 ms
EPI factor	64

Raw images and all derived images from following analysis steps were visually inspected at all stages to ensure quality control. Initially, the raw 2D DICOM (Digital Imaging and Communications in Medicine) files outputted from the scanner were converted into 3D/4D NIFTI (Neuroimaging Informatics Technology Initiative) images making use of the converter tool from Neuroimaging Tools & Resources Collaboratory (NITRC nitrc.org/projects/mricrogl). The imaging datasets were organised according to the Brain Imaging Data Structure (BIDS), a validated standard for organizing, describing and sharing MRI datasets [48]. Structural images (T1-weighted and T2-FLAIR) were brain extracted using FSL's BET (brain extraction tool), manually cropping and adjusting parameters for the best fit [49].

2.6.1 MRI distortions correction

MRI, as a non-invasive imaging method, records the brain signal indirectly and thus scans are highly prone to carry multiple kinds of noise-induced distortions. Distortions might not have a great impact on clinical diagnosis, however, they can easily compromise the existence or validity of statistical results. As such, the first step of every analysis is to, as best as possible, account for these errors. In the aim of this study, we focused on four main sources of distortions:

- bias field;
- susceptibility distortions;
- eddy currents;
- and motion.

Bias field is a low frequency smooth signal that is originated due to the lack of homogeneity of the main magnetic field of the scanner. It blurs k-space and thus reduces the images' high frequency contents and changes the intensity values of voxels of the same tissue across the image. Moreover, it degrades the performance of imaging processing algorithms (e.g. those based on the assumption of spatial invariance of the image) [50]. For this, FMRIB's Automated Segmentation Tool (FAST) was used. FAST, besides segmenting a 3D image of the brain into different tissue types (grey matter, white matter, CSF, etc.) and also corrects for spatial intensity variations [51].

When a patient lies in the bore of the scanner, the structure of the brain generates magnetic field inhomogeneities (especially near boundaries between skull and the air sinuses located around the nose). These local changes in the magnetic field strength are problematic when acquiring EPI data. The field inhomogeneities interact with the expected signal and can therefore lead to signal loss in some areas (dropout) or signals ending up in the wrong location (aliasing). This distortion can be solved by realigning the data using field maps. The protocol used for this study did not contain field maps and thus a solution a replacement image was created using FSL's TOPUP [52], [53]. It uses two dMRI acquisitions where the phase encoding directions are opposite, such that the same field inhomogeneity will lead to distortions going in opposing

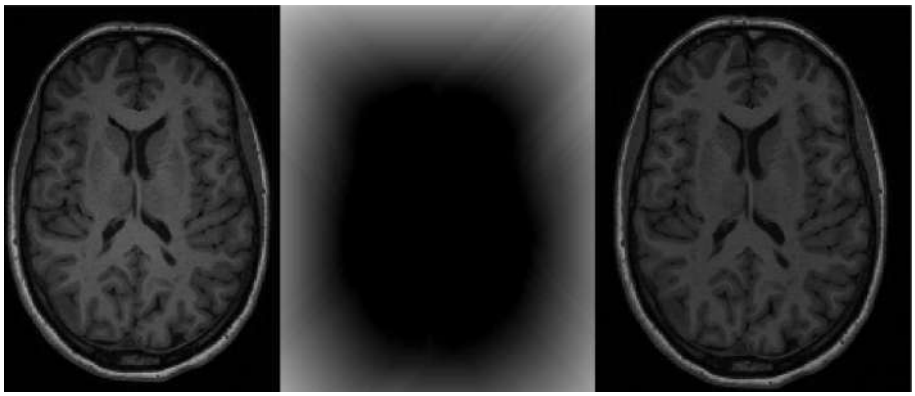

FIGURE 2.3: Example of bias field correction. On the left it is shown a T1-weighted image with presence of bias field (grey matter can be seen with different intensities in the left and right side of the image); the centre represents the bias field and, on the right, it is shown the same T1-weighted image corrected for the bias field.

directions. This tool will estimate an off-resonance field by finding the field that when applied to the two volumes will maximise the similarity of the unwarped volumes.

Electrical current is induced in nearby conductors by a changing magnetic field. Since MR uses rapidly changing magnetic fields to generate and spatially define the signal, eddy currents are produced. Thus, imaging sequences where gradients are pulsed on and off quickly (dMRI) produce the largest and most severe eddy current problems. Such artefacts are removed using FSL's eddy tool [54]. Lastly, head motion was identified and corrected for fMRI images using FSL's MCFLIRT - a fully automated robust and accurate tool for linear inter- and intra-modal brain image registration [55].

2.6.2 White matter hyperintensity load extraction

As described above, one big feature of cerebral SVD is the widespread white matter damage (white matter hyperintensities – WMHs). WMHs are areas of increased brightness when visualised by T2-weigthed imaging (hence hyperintensities). Although WMH have been associated with reduced cognitive function, it's role in SVD is still unclear. Thus, for this study, we want to be able to control for WMH load in the structural and functional analysis. For this, extracting the total WMH load for all subjects was needed. FMRIB's tool for automated segmentation of white matter hyperintensities (BIANCA) was used. BIANCA is an automated, supervised method to detect white matter hyperintensities (WMH). Its algorithm is based on the k-nearest neighbour (k-NN) clustering technique. BIANCA classifies the image's voxels based on their intensity and spatial features, and the output image represents the probability per voxel of being WMH [56]. To fully run said pipeline, training points from a previous study on small vessel disease was used. This study used a very similar cohort, in the same scanner with a similar sequence. These factors make the features extracted from the study appropriate for this

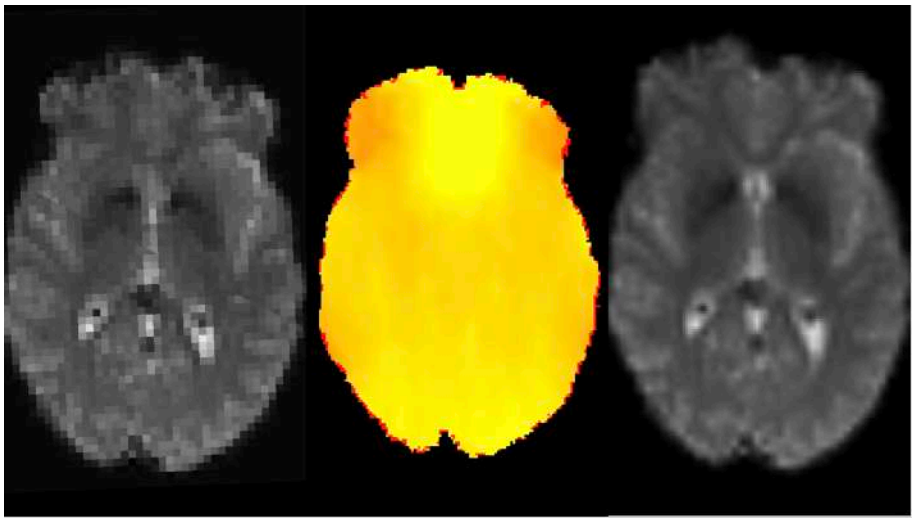

FIGURE 2.4: Example of susceptibility correction on functional MRI data by applying a field map. On the left it is shown an uncorrected fMRI volume. The centre represents that off-resonance field generated by TOPUP. On the right is shown the same fMRI volume corrected for susceptibility distortions.

study. BIANCA ouput individual lesion probability maps for each subject. Then, these maps are manually thresholded to best fit the lesion of each subject. To ensure the quality of the lesion masks, the thresholding was done by two raters (one with basic knowledge of WMH and by a fully trained medical doctor). Cases of ambiguity were to be discussed with a more senior medical professional.

2.6.3 Tract Based Spatial Statistics

Diffusion imaging offers methods for the investigation of white matter tract integrity. In specific, fractional anisotropy (FA) has been shown to, in previous studies, be a potential marker of

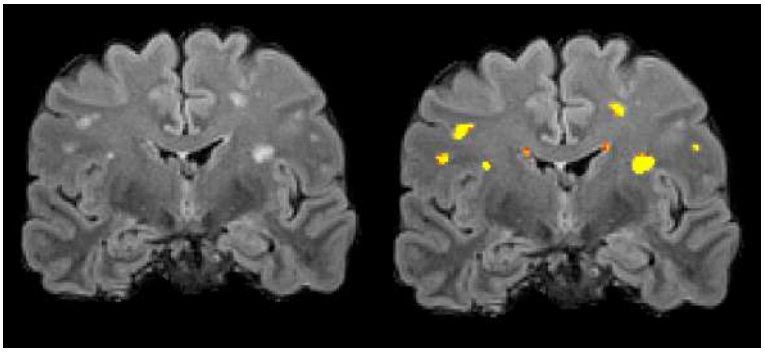

FIGURE 2.5: Example of the application and thresholding of the BIANCA lesion probability map. On the left it is shown a coronal slice of the T2-weighted FLAIR image and on the right, the same slice with application of the lesion mask (in yellow).

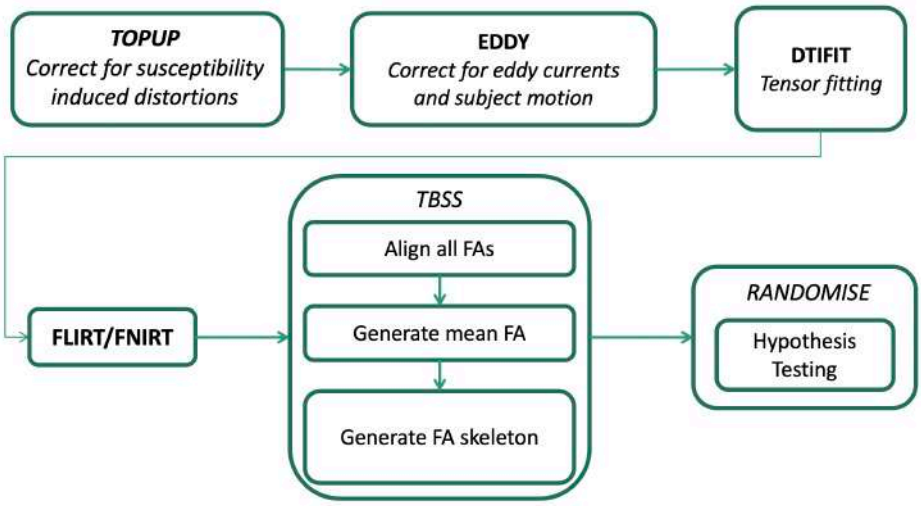

FIGURE 2.6: TBSS dMRI pipeline.

structural integrity and white matter damage [57], [58]. In this study, to compare structural integrity of white matter between apathetic and non-apathetic cerebral SVD patients, voxelwise statistical analysis of the FA values was carried out using TBSS (Tract-Based Spatial Statistics, part of FSL). First, FA images were created by fitting a tensor model to the raw diffusion data using FDT, and then brain-extracted using BET. All subjects' FA data were then aligned into a common space using the nonlinear registration tool FNIRT, which uses a b-spline representation of the registration warp field. Next, the mean FA image was created and thinned to create a mean FA skeleton which represents the centres of all tracts common to the group [53], [59].

Each subject's aligned FA data was then projected onto this FA skeleton and the resulting data fed into a GLM, in which t-tests to compare the changes in FA between groups. T-stats were corrected using TFCE (threshold-free cluster enhancement) [60]. In the GLM, regressors of no interest are introduced as covariates [61].

2.6.4 Voxel-based morphometry

Structural data was analysed with FSL-VBM (voxel-based morphometry) [62], an optimised VBM protocol [63] carried out with FSL tools. First, structural images were brain-extracted and grey matter-segmented before being registered to the MNI 152 standard space using non-linear registration. The resulting images were averaged and a study-specific grey matter template was generated. After, all original structural images were non-linearly registered to this study-specific template and corrected for local expansion (or contraction) due to the non-linear component of the spatial transformation with the output Jacobian matrix. The modulated grey matter images were then smoothed with an isotropic Gaussian kernel with a sigma of 3 mm. The resulting subject-wise grey matter images were fed into a voxelwise GLM, in which t-tests to

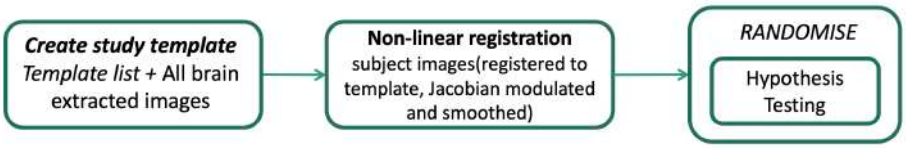

FIGURE 2.7: VBM structural pipeline.

compare the changes in grey matter volume between groups. T-stats were corrected using TFCE (threshold-free cluster enhancement) [60]. In the GLM, regressors of no interest are introduced as covariates [61].

2.6.5 fMRI denoising

The fMRI data was pre-processed using FSL's MELODIC (Multivariate Exploratory Linear Decomposition into Independent Components) [64]. MELODIC uses Independent Component Analysis (ICA) to decompose a 4D data into different spatial and temporal components. MELODIC uses a probabilistic ICA (pICA)model formulated as a generative linear latent variable model. The model assumes that the observations are generated from a set of statistically independent non-Gaussian sources via a linear instantaneous mixing process corrupted by additive Gaussian noise:

$$X = AS + \mu + n \tag{2.1}$$

Here, X denotes individual measurements at voxel location, S denotes the non-Gaussian source signals contained in the data, μ the mean of the observations X and lastly, n the Gaussian noise. The covariance of the noise is allowed to be voxel dependent in order to allow for the vastly different noise covariances in different tissue types. The pICA model is similar to the standard GLM with the difference that, unlike the design matrix in the GLM, the mixing matrix A is no longer pre-specified prior to model fitting. The source signals are the equivalent to the GLM parameter estimates, but with the additional constraint of being statistically independent. In MELODIC, the problem of defining the dimensionality of the ICA is solved by prior running PCA (principal component analysis). PCA is a similar method to ICA, but instead of looking for statistical independence in the components, PCA looks for orthogonal components to each other and that explain the maximum amount of variance in the data. In here, PCA is run and after, the number of components chosen for the ICA decomposition is defined by the number of the PCA component after which no more variance is explained.

The parameters of this imaging pre-processing pipeline used on all participants are as follow: motion correction using MCFLIRT, non-brain removal using BET, spatial smoothing using a Gaussian kernel of FWHM 5mm; grand-mean intensity normalization of the entire 4D dataset

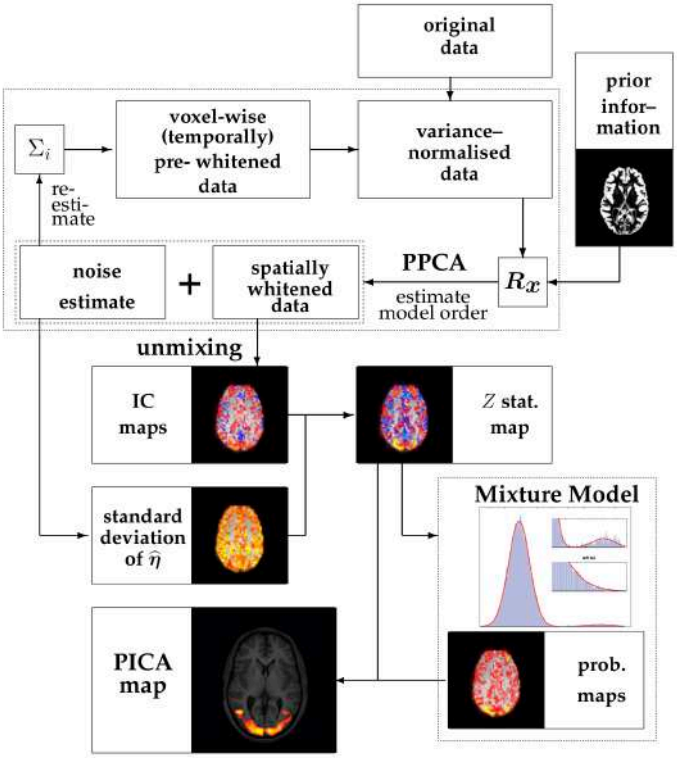

FIGURE 2.8: Schematic illustration of the analysis steps involved in estimating the pICA model. Taken from [64].

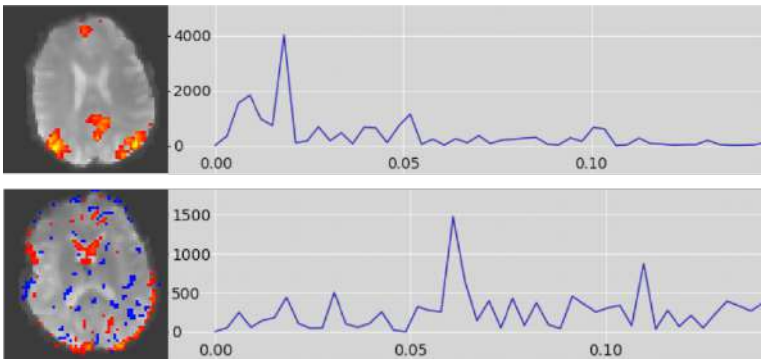

FIGURE 2.9: ICA decomposition. Above it is shown the spatial distribution and power spectrum of a signal component (coactivation of DMN areas and a frequency distribution mostly below 0.1 Hz). Below, it's shown the spatial distribution and also the power spectrum of a noise component (wide power spectrum and spatial features common of motion artefacts and CSF pulsation).

by a single multiplicative factor and linear detrending over 50 second intervals, B0 unwarping using the field maps developed, slice timing correction making use of the slice timing from the fMRI metadata, high pass temporal filtering (using a local fit of a straight line) to remove low frequency artefacts and registration between functional and structural space using FSL's FLIRT. Manual classification of the output independent components between "signal" and "non-brain" was conducted following published guidelines [65]. Components identified as "non-brain" were regressed out of the fMRI data using fsl_regfilt.

2.6.6 Dual Regression Analysis

Firstly, functional connectivity was analysed under a static assumption (i.e. averaging the BOLD signal over the whole acquisition time). In order to statistically detect differences in resting state networks between groups of subjects, the individual ICA components could be used. However, in practice, it's often the case that a network will be described by a single component in one subject but split in two (or more) separate components in another subject (i.e. there is a correspondence problem). Therefore, a more practical approach is to run a group analysis in order to ensure that the components are the same across all the subjects, and then map these group components back to individual subjects. To address this problem, the dual regression FSL pipeline was employed. The dual regression uses group-ICA maps (generated by running multi-session temporal concatenation MELODIC) and applies two subsequent regression analyses using the original pre-processed dataset from each subject in order to derive subject-specific maps. The first stage of a dual regression analysis is to perform a multiple regression analysis where the group-ICA maps are the spatial regressors, and the subject's pre-processed BOLD dataset is the input data (dependent variables). The result of this first stage of dual regression is a set of timecourses (one for each group map) that describe the temporal structure of each component for each subject. These timecourses then become the model for the second

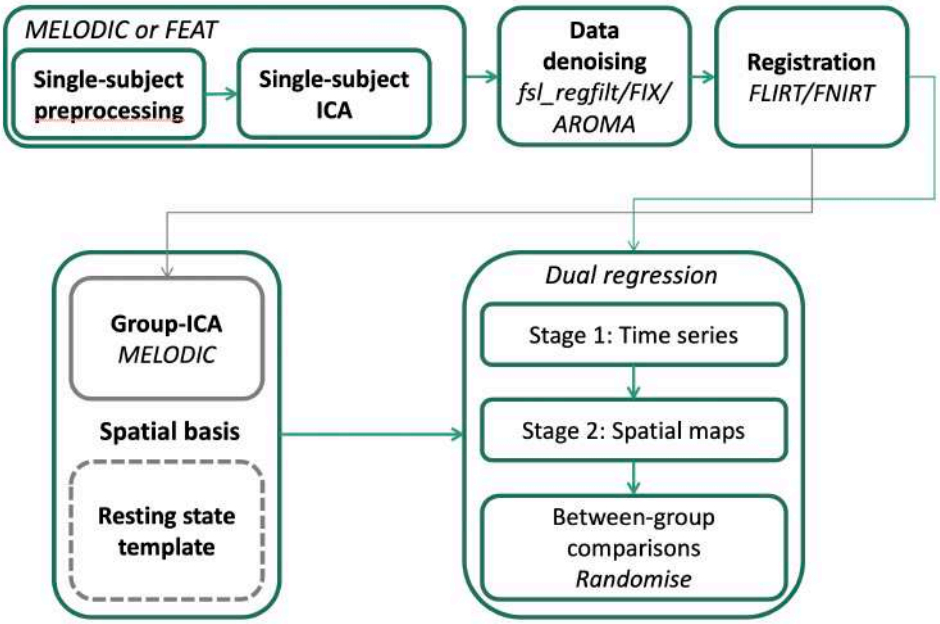

FIGURE 2.10: Dual regression fMRI pipeline.

stage of the dual regression. This second stage involves a second multiple regression, where the temporal regressors of the first stage are regressed against the subject's pre-processed BOLD data. The output is then a set of maps (one for each original group-ICA component) that describe the network structure based on the data from each subject [66].

These group-ICA maps for each subject are then used for between-group analysis. A GLM is built to assess the differences in mean activation between groups. T-stats were corrected using TFCE (threshold-free cluster enhancement) [60]. In the GLM, regressors of no interest are introduced as covariates [61].

2.6.7 Leading Eigenvector Dynamics Analysis (LEiDA)

Secondly, functional connectivity analysis was conducted in order to capture the BOLD fluctuations at all timepoints. For this, the single-level denoised fMRI datasets were used. We used the Anatomical Automatic Labelling (AAL) atlas to parcellate the MNI brain into 90 cortical and sub-cortical brain areas. The BOLD signals were then averaged over AAL brain regions using FSLUTILS. To compute the phase coherence between the of AAL regions, first the BOLD phases, $\theta(n,t)$, were estimated using the Hilbert transform for the timecourse of each AAL region. The Hilbert transform expresses a given signal x as $x(t) = A(t) * cos(\theta(t))$, where A is the amplitude and θ is the phase (both varying with time). Literature has shown that $cos(\theta(t))$ captures the oscillatory dynamics of the original BOLD signal with constant amplitude. To obtain the pattern of phase coherence at each single time point t, we compute a dynamic phase

coherence matrix $dPC(n, p, t)$ which estimates the phase coherence between brain areas n and p at time t, using:

$$dPC(n, p, t) = cos(\theta(n, t) - \theta(p, t)) \tag{2.2}$$

Using the cosine function, two areas n and p with temporarily aligned BOLD signals (i.e. with no phase difference) at a given TR will have a phase coherence value of 1. On the other hand, time points where the BOLD signals have 180 degree phase difference (in the complex plane) will have a value of -1. The resulting dPC for each subject is thus, a three-dimensional matrix with size, NxNxT, where N=90 is the number of brain areas and T=200 is the total number of time points. To characterise the evolution of the dPC matrix over time, we employed a method termed Leading Eigenvector Dynamic Analysis (LEiDA) focusing on the evolution of the dominant pattern of the phase coherence over time. The leading eigenvector of the phase coherence matrix at time t, V1(t) represents the projection of the BOLD phase in each brain area into the leading eigenvector. When all elements of V1(t) have the same sign, it means all BOLD phases are following the same direction with respect to the orientation determined by V1(t), which is indicative of a global mode governing all BOLD signals. If instead, the first eigenvector V1(t) has elements of different signs (i.e. positive and negative), the BOLD signal follows different directions with respect to the leading eigenvector, which we use to divide the brain areas into two "communities" according to their BOLD phase relationship. Moreover, the magnitude of each element in V1(t) indicates the "strength" with which brain areas belong to the communities in which they are placed. To identify recurrent phase coherence (PC) patterns we used a clustering algorithm (k-means) to divide the sample of PC eigenvectors (3200 vectors corresponding to all 200 TRs of 18 CADASIL patients and 13000 vectors corresponding to all 200 TRs of 65 sporadic SVD patients) into a predefined number of clusters k (with higher k revealing rarer and more fine-grained patterns). Since the optimal number of functional networks to consider remains an open question, we ran the k-means clustering algorithm with k ranging from 5-15 to cover the range of functional networks commonly reported in the resting state fMRI literature. Importantly, in the current study we do not aim to determine the optimal number of PC states, but rather to investigate if there are PC state(s) that differ in their probability of occurrence over this range in apathetic and non-apathetic SVD patients. For each partition model (i.e. $k = 5$ to $k = 15$), the clustering returns k cluster centroids in the shape of Nx1 vectors, Vc, which represent the central vector of each cluster. We take these central vectors as representing recurrent states of BOLD phase coherence, or PC states. To facilitate visualisation and interpretation of PC states, the cluster centroid vectors Vc obtained were rendered onto a cortical surface using SPM12. The clustering assigns to each TR a single PC state by selecting the centroid Vc that is closer to the V1(t) at each TR. Using the state time course, we calculated the probability of occurrence of each state, which is simply the number of epochs assigned to a given PC state divided by the total number of epochs (TRs) in each scan. For each partition mode (i.e. with $k = 5$ to $k = 15$) the probabilities of each PC state were calculated for each

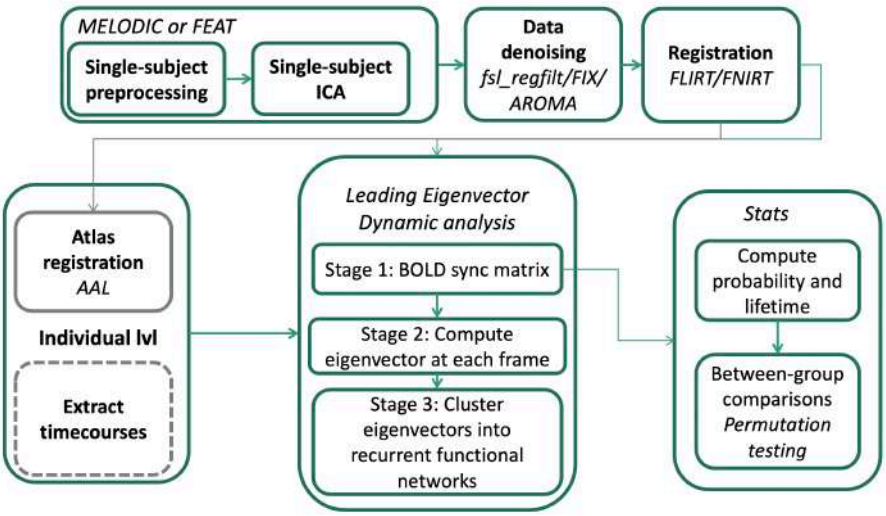

FIGURE 2.11: Leading Eigenvector Dynamics Analysis (LEiDA) pipeline.

group (apathetic and non-apathetic SVD patients).

2.6.8 Statistical thresholding

A common statistical problem in neuroimaging studies (that occurs in relation to null hypothesis testing) is the multiple comparison problem. When we perform a large number of tests it is essential to apply some form of correction to control the number of false positives accepted. This study uses, for the VBM, TBSS and static functional connectivity analysis (dual regression), a family-wise error rate correction, which is the standard correction method. For the LEiDA analysis (functional connectivity dynamics), where we're testing only at the level of the parcellation scheme and not voxel per voxel, a more stringent correction is applied (Bonferroni correction).

2.7 Statistical analysis of the data

2.7.1 Cognitive assessment statistics

To check the effect of apathy on the cognitive function, depression and quality of life in the cerebral SVD populations, the scores of the cognitive questionnaires were tested through one-way ANOVAS (groups defined by apathy classification described above).

2.7.2 Behavioural experimental statistics

Data from the behavioural paradigm was analysed in a couple of separate ways. Firstly, we looked at raw proportion of offers accepted with a one-way ANOVA. Secondly, a repeated measures ANOVA was used to test whether the proportion of accepted trials per condition varied as function of reward, effort, apathy or their interactions. Lastly, a computational model (glme – general linear mixed-effect model) was used to estimate, for each participant, the degree that reward and effort changed the value of an effort. The model was selected based on a comparison of candidate models from the literature [67], [68], using standard minimisation of the Bayesian information criterion. An exponential model closely approximated both individual and average raw choices:

$$value = \alpha.Reward.exp(-\beta.effort + k) \tag{2.3}$$

Where α estimated the degree to which reward increased the value of an offer, β estimated the degree to which effort reduced the value of an offer and k the baseline tendency to accept an offer. Parameters were normally distributed and therefore compared using independent t-tests.

2.7.3 Imaging statistics

For all the imaging analysis (across all modalities), the CADASIL and sporadic SVD groups were always tested separately, with the objective of establishing relations between the groups. Regressors of no interest were always demeaned before being input to the GLM, as to still account for their variance within the data, but not their mean. GLM statistics were always corrected for multiple comparisons and with TFCE. Grey matter estimates outputted from VBM, TBSS FA estimates and dual regression's components were analysed making use of two GLMs. Both of them tested only for one contrast: mean of the non-apathetic group > mean of the apathetic group. GLMs varied between one another only in the number of covariates added. The first controlled for age and sex. The second controlled for age, sex and white matter load. Differences in probabilities of occurrence between groups of phase coherence states from LEiDA were statistically assessed using a permutation-based paired t-test. This non-parametric test uses permutations of group labels to estimate the null distribution, which is computed independently for each group. For each of 1000 permutations a t-test is applied to compare populations and a p-value is returned.

2.7.4 Combined neuroimaging and behavioural statistics

Parameter estimates of reward and effort sensitivity were compared with grey matter volume estimates from VBM, FA values extracted from TBSS and the state probabilities from LEiDA, making use of the Pearson correlation and its statistic significance assessed with t-tests.

3 Results

3.1 Apathetic behaviour

As part of the core testing for this project, both the CADASIL and sporadic SVD populations completed several questionnaires aiming at assessing multiple aspects of their life (Table 3.1, Table 3.2). With these questionnaires we aimed at depression, cognitive function and quality of life, and if they show any association with apathy.

To test whether apathy was affecting cognitive function, quality of life and depression, the ACE, CANTRIL ladder and BDI scores of the CADASIL and the sporadic SVD groups were analysed with one-way ANOVAs. This statistical test would compare whether the mean values for each group would be significantly different. After the ANOVA was computed, using R, the boxplots of the questionnaire score and their distribution across apathetic and non-apathetic group was created. The boxplots contain the distribution (mean, median and quantiles) of the apathetic (on the right) and non-apathetic (on the left), of both populations (CADASIL and sporadic SVD) for all the relevant questionnaires (Figure 3.1,Figure 3.2, Figure 3.3).

In both populations, the apathetic group has shown reduced cognitive function (as assessed by the ACE-III) when compared to the non-apathetic patients.

While the CADASIL group shown no significant difference in cognitive function ($F = 2.55$, $p = 0.1311$), there was an effect of apathy in the cognitive function of the sporadic SVD patients ($F = 7.45$, $p = 0.0083$).

Table 3.1: Results of the cognitive assessment questionnaires of the CADASIL group

Measure	CADASIL (n=18)	No apathy (n=8)	Apathy (n=10)
LARS (range -36:36)	-20.6 ± 11.9	-29.0 ± 3.5	-13.8 ± 11.9
AES (range 0:72)	34.9 ± 10.6	25.8 ± 5.6	41.4 ± 9.1
GDS (range 0:15)	5.4 ± 4.9	2.1 ± 2.5	8.3 ± 4.8
Cantril (range 0:10)	6.7 ± 2.2	8.0 ± 0.8	5.7 ± 2.3
BDI	10.8 ± 12.7	2.8 ± 2.9	17.7 ± 14.1
ACE-III	92.5 ± 5.3	94.8 ± 2.4	90.6 ± 6.3

TABLE 3.2: Results of the cognitive assessment questionnaires of the sporadic SVD group

Measure	Sporadic SVD (n=104)	No apathy (n=59)	Apathy (n=45)
LARS (range -36:36)	-21.7 ± 7.3	-26.3 ± 3.2	-15.6 ± 6.7
AES (range 0:72)	31.8 ± 8.7	27.3 ± 4.9	37.5 ± 9.2
Cantril (range 0:10)	7.2 ± 1.7	7.7 ± 1.6	6.5 ± 1.7
BDI	10.8 ± 8.0	8.6 ± 5.9	13.7 ± 9.3
ACE-III	88.4 ± 12.6	91.7 ± 7.1	84.0 ± 16.5

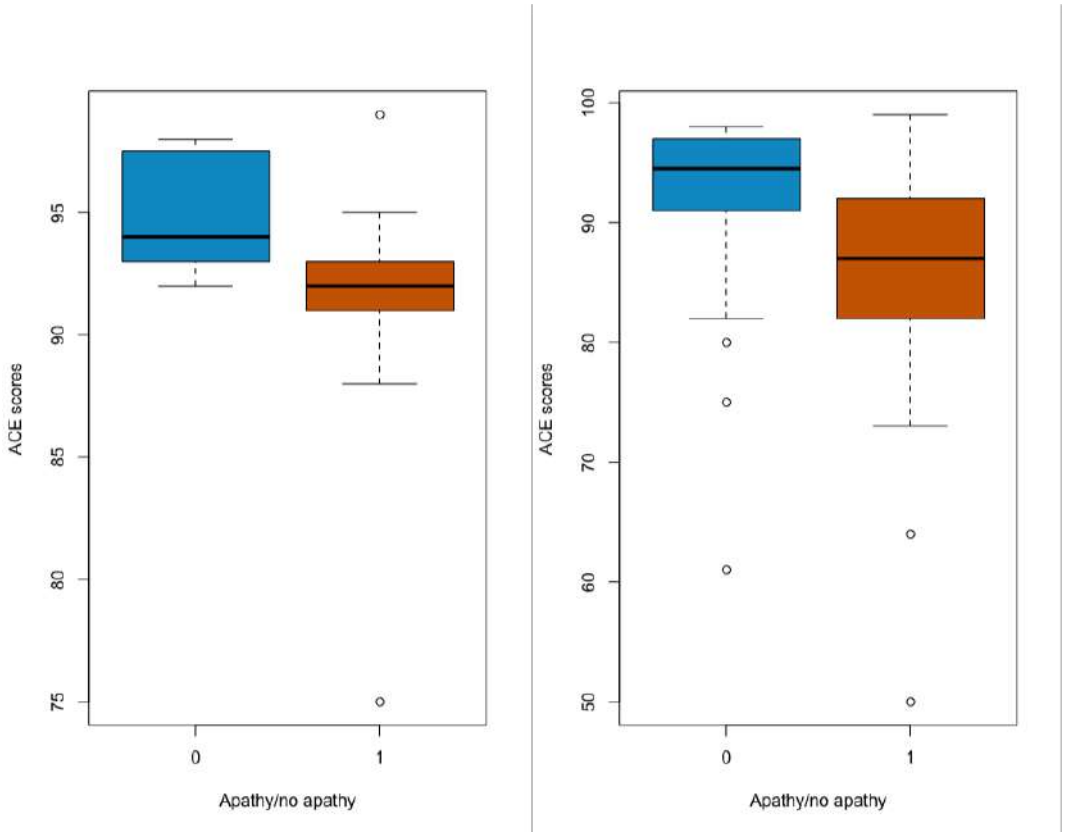

FIGURE 3.1: Boxplot of the ACE scores divided by apathetic and non-apathetic groups. On the y-axis there's the ACE scores. Right: CADASIL, Left, sporadic SVD.

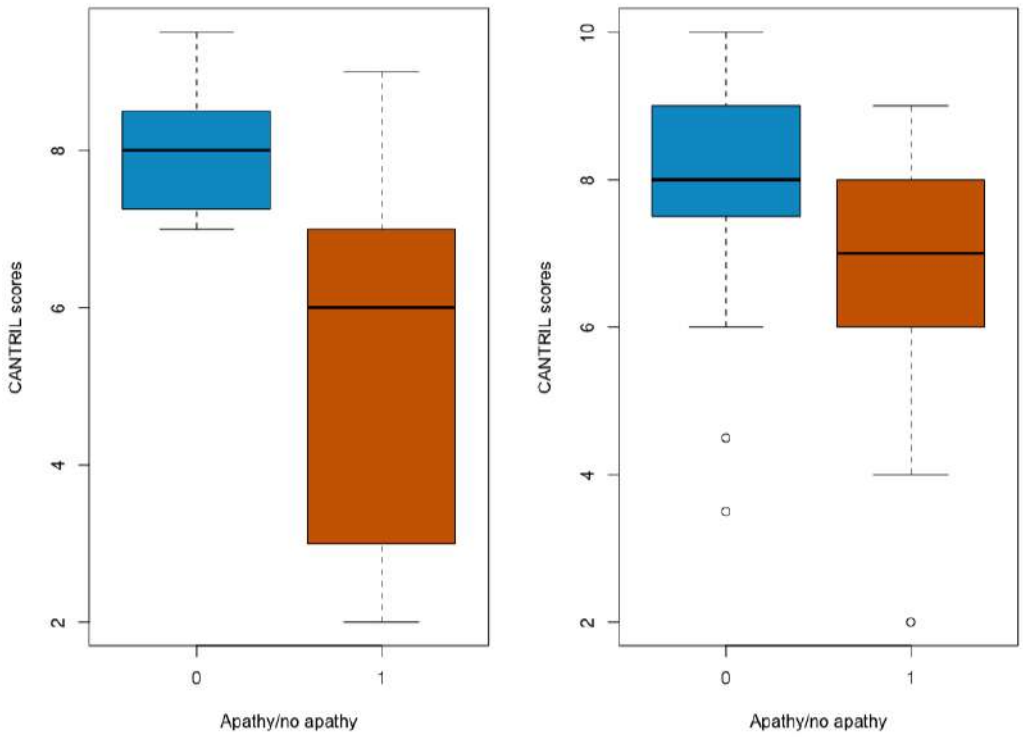

FIGURE 3.2: Boxplot of the Cantril scores divided by apathetic and non-apathetic groups. On the y-axis there's the Cantril scores. Right: CADASIL, Left, sporadic SVD.

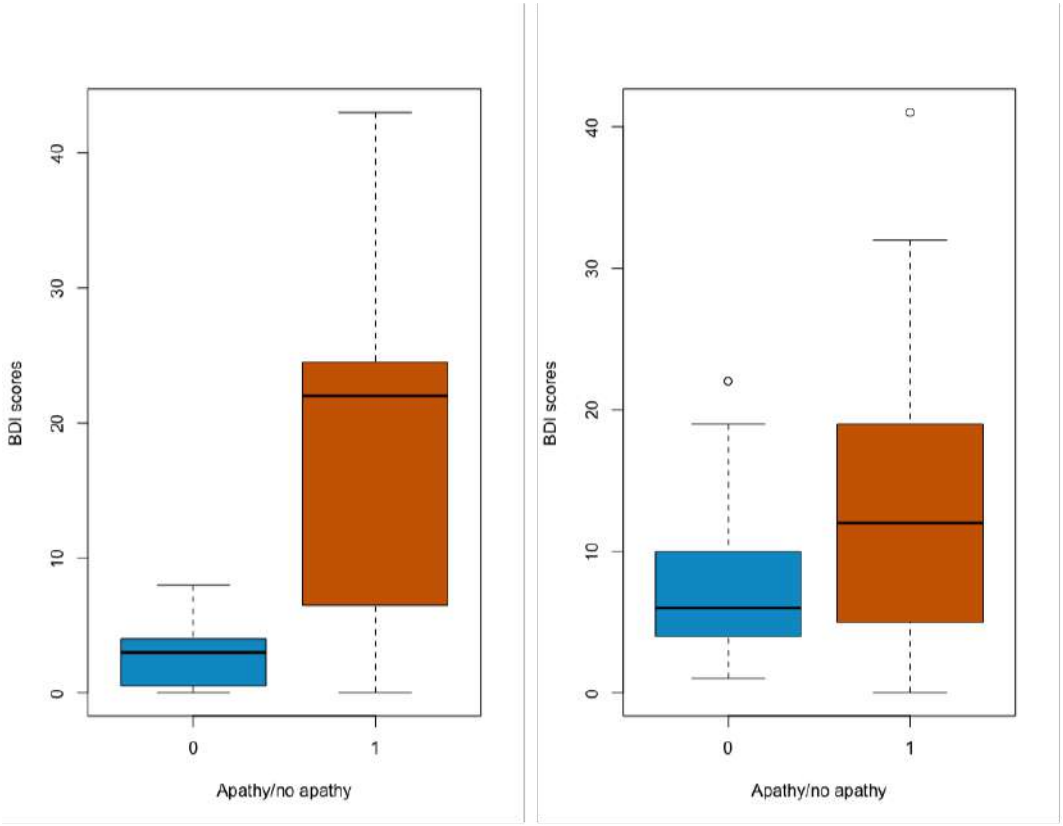

FIGURE 3.3: Boxplot of the BDI scores divided by apathetic and non-apathetic groups. On the y-axis there's the BDI scores. Left: CADASIL; Right, sporadic SVD.

Both the CADASIL and the sporadic SVD apathetic populations shown significantly lower quality of life in comparison to their non-apathetic counterpart ($F = 6.47$, $p = 0.0225$; $F = 12.28$, $p = 0.0009$ respectively). This further demonstrates the already widely studied degradation of life caused by apathy.

Moreover, both populations (CADASIL and sporadic SVD), apathetic patients appear to be more depressed then their non-apathetic counterparts (possibly associated with the decreased quality of life reported). This effect is significant for both populations(CADASIL: $F = 6.86$, $p = 0.0224$; sporadic SVD: $F = 20.91$, $p = 2.36e - 05$).

After having better insight into our populations, we also wanted to look with greater detail on the apathy classification system. Apathy was assessed using two questionnaires, filled subjectively by each participant. We wanted to infer whether questionnaires were classifying the patients similarly. We've then looked at the correlation between both individual scores with the aim at ensuring the validity of the participants answers and thus, the apathetic/non-apathetic group division.

In both populations, we have a good linear fit of the both questionnaires. Both associations

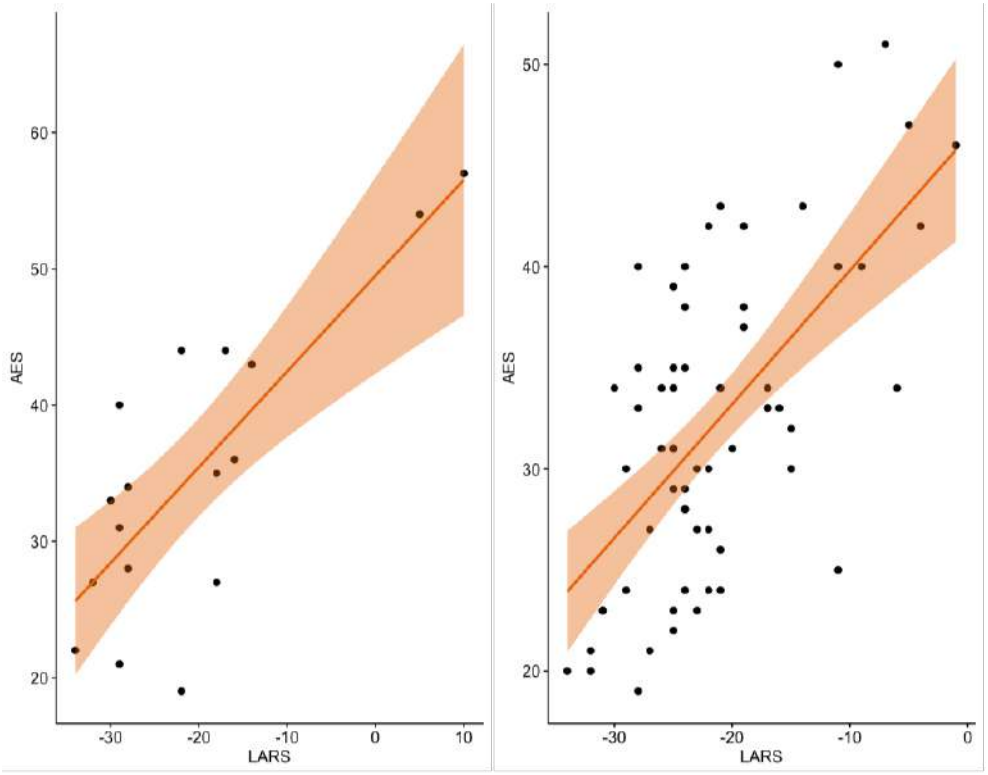

FIGURE 3.4: Plot of the Pearson correlation between the scores of the LARS and AES of each individual patient. On the x-axis are the apathy evaluation (AES) scores and on the y-axis, the Lille apathy rating scale (LARS) scores. The orange band around the regression line is the confidence interval. Left: CADASIL, Right: sporadic SVD.

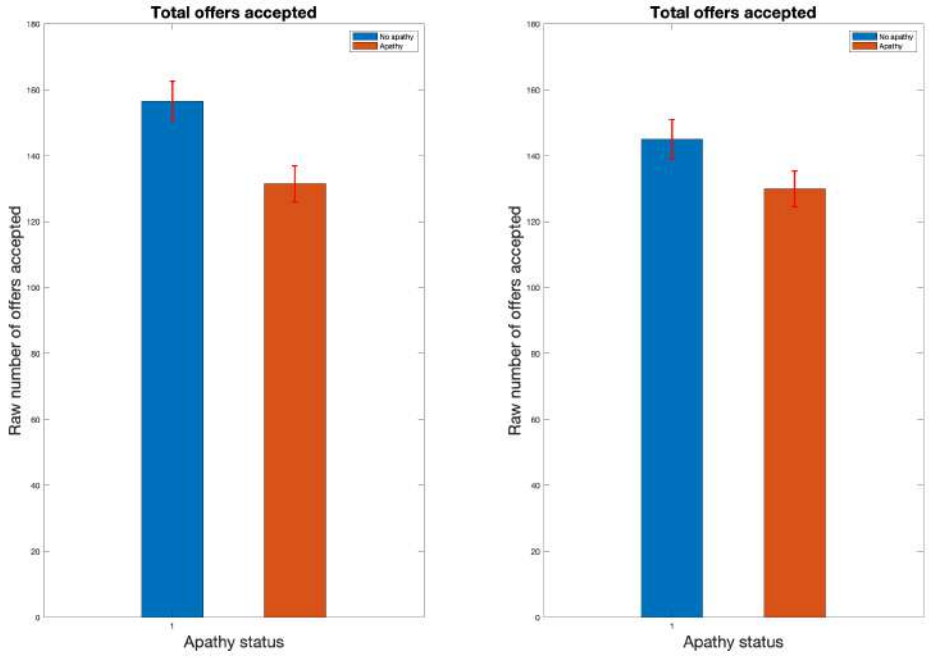

FIGURE 3.5: Proportion of offers accepted across the whole experiment by the apathetic and non-apathetic groups. Left: CADASIL, Right: sporadic SVD.

are positive, meaning that an increase in apathy measured with one questionnaire was assessed equally by the other. In the CADASIL population, the scores of both questionnaires are positively associated with each other ($r - squared = 0.62$, $p = 0.00017$). In the sporadic SVD group the positive association isn't as strong, but still significant ($r - squared = 0.39$, $p = 2.68e - 08$).

After, we aimed at understanding how the diagnosed apathy would impact behaviour on the decision-making task. Thus, we compared the proportion of total accepted offers and their cumulative acceptance across the experiment. We've analysed the acceptance rate in the two groups using a one-way ANOVA.

Both populations show a difference in their overall offer acceptance. Apathetic patients accept fewer offers than non-apathetic. However, CADASIL patients with apathy accepted significantly fewer offers than patients without apathy ($F = 4.85$, $p = 0.0418$) and this effect was not seen in the sporadic SVD (unless the effect of depression would be regressed out).

To investigate the factors driving reduced acceptance of offers in the apathetic group, we used a repeated measures ANOVA to analyse how the proportional acceptance rate in each cell of the sampled 6x6 decision space varied with reward, effort and apathy.

The difference was not global across the sampled decision space. It varied with reward but not effort. There was a significant two-way interaction between apathy and reward, but not between apathy and effort. This shows that patients rejected significantly more offers when reward

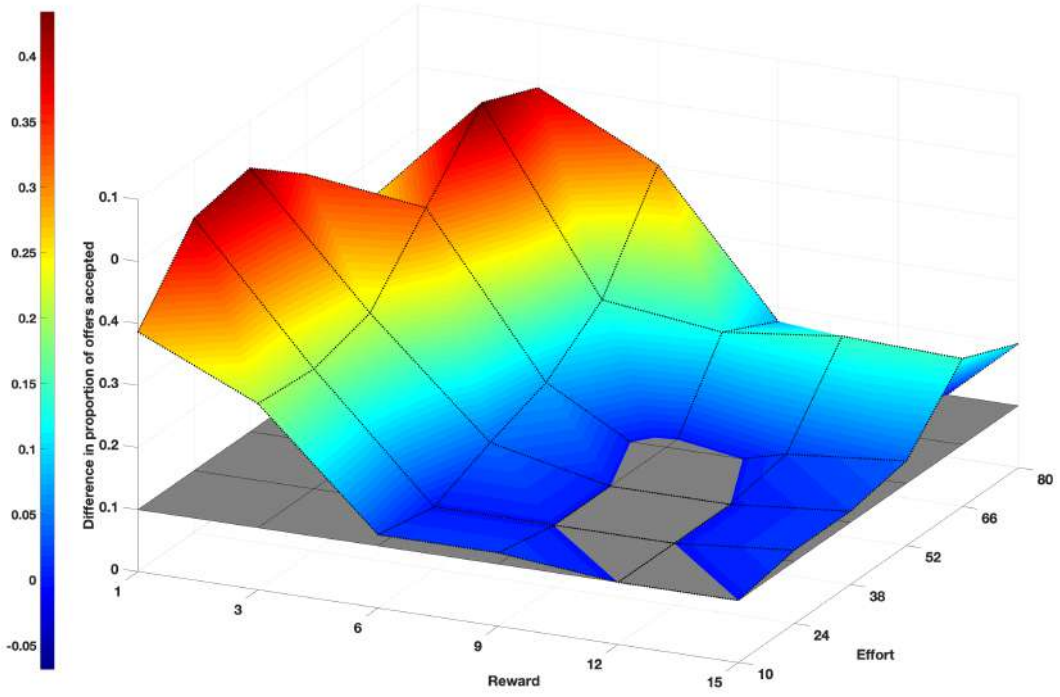

FIGURE 3.6: The difference in offers accepted between apathetic and non-apathetic patients across decision space.

TABLE 3.3: Computational modelling parameter estimates of the CADASIL patient group.

Measure	CADASIL (n=18)	No apathy (n=8)	Apathy (n=10)
Reward sensitivity	-1.66 ± 8.89	-2.63 ± 1.85	-0.58 ± 13.21
Effort sensitivity	2.14 ± 1.22	1.48 ± 0.93	2.87 ± 1.12

TABLE 3.4: Computational modelling parameter estimates of the sporadic SVD patient group.

Measure	Sporadic SVD (n=83)	No apathy (n=47)	Apathy (n=35)
Reward sensitivity	-0.44 ± 2.86	-0.77 ± 2.66	0.04 ± 3.10
Effort sensitivity	-0.07 ± 0.66	-0.14 ± 0.58	0.03 ± 0.74

was low, but showed no difference compared to non-apathetic patients at high reward levels, irrespective of what the effort costs were. There were also significant main effects of apathy, and a two-way interaction between reward and effort. There was no three-way interaction between apathy, reward and effort.

Next, we compared the parameter estimates for reward (α), effort (β) and intercept (k) obtained from the computational model of choice fitted to each participant's decisions. Modelled data closely approximated raw choice data, both for each CADASIL patient and for group average choice proportions.

Both parameter estimates of the apathetic CADASIL group are reduced when compared to their counterparts. Through statistical analysis, significant difference was found in effort sensitivity ($F = 7.76$, $p = 0.0138$) but the same significant effect was not found for reward sensitivity.

From the computational modelling of the sporadic SVD behavioural data, no significant difference was found in either of the parameters.

3.2 Tract-based spatial statistics

Literature has shown that reduced integrity of white matter in key tracts (represented by reduced FA - fractional anisotropy) seems to be associated with apathetic behaviour. We then wanted not only to confirm these findings in our populations but also to understand if our populations were affected in different white matter tracts. We've then began our image analysis by identifying the areas of reduced white matter integrity in the apathetic groups versus their non-apathetic counterparts using TBSS in both CADASIL and sporadic SVD. This methodology fits a tensor on all identified white matter voxels and estimates an FA measure for it. The mean FA skeletons of each subject are then registered to standard space, where voxelwise statistics are done.

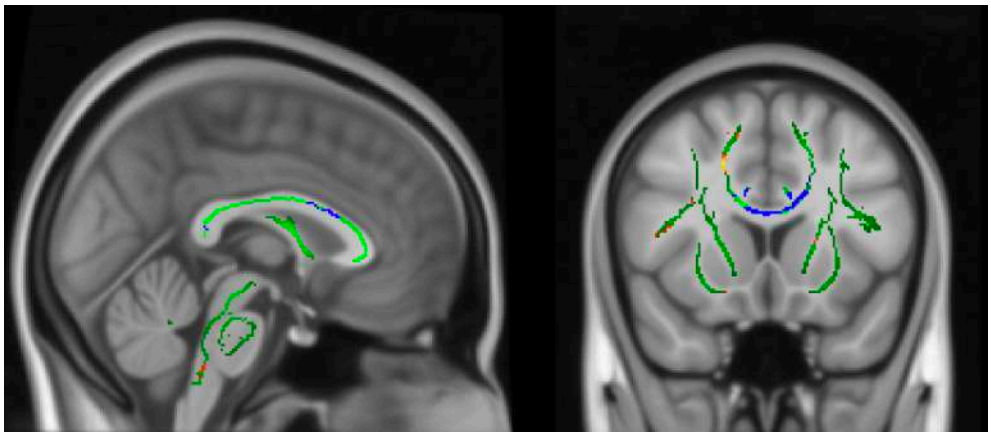

FIGURE 3.7: TBSS results of CADASIL: Sagittal and transversal slices of the MNI 152 template. $P < 0.1$, TFCE-corrected in blue, against the study-specific FA skeleton in green. Apathetic CADASIL patients show significantly reduced white matter FA when compared to non-apathetic patients within the right and left anterior cingulum, and parts of the corpus callosum.

TBSS results of the CADASIL population show that apathy is associated with a reduction of white matter FA within regions of the anterior cingulum and the body of the corpus callosum (Figure 3.7). Very similar results seem to be found in the sporadic SVD population (Figure 3.8). The reduced white matter FA is more spread out in the corpus callosum of the sporadic SVD, however, no association with apathy is seen in its splenium.

3.3 Voxel-base morphometry

After identifying the brain regions of reduced integrity, at whole brain, we studied the changes of grey matter volume associated with apathy and what could be the relation between those and the ones of reduced white matter integrity (reduced FA). This was achieved by running the VBM pipeline on the cerebral SVD populations. This method estimates the grey matter volume of all subjects, generates a study template to which all grey matter subject masks are registered to. Then, voxelwise statistics are done on it.

VBM results of CADASIL show that apathetic patients have a significantly reduced grey matter volume in areas of the occipital lobe when compared to their non-apathetic counterparts (Figure 3.9). However, in spite of the sporadic SVD population showing a similar change, it's not statistically significant.

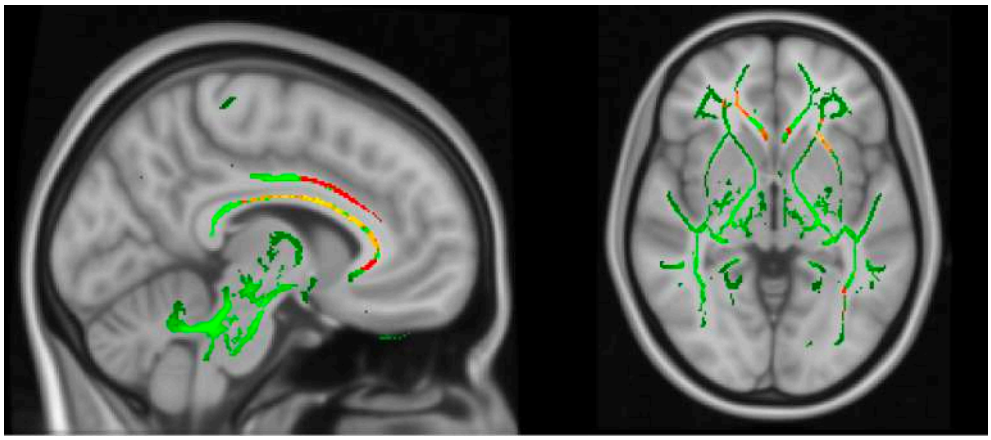

FIGURE 3.8: TBSS results of sporadic SVD: Sagittal and transversal slices of the MNI 152 template. P < 0.1, TFCE-corrected in blue, against the study-specific FA skeleton in green. Apathetic sporadic SVD patients show significantly reduced white matter FA when compared to non-apathetic patients within the right and left anterior cingulum, and parts of the corpus callosum.

3.4 Functional connectivity

MELODIC ICA decomposed the fMRI dataset of the cerebral SVD populations into 100 statistically independent components. Looking at the components we were able to identify several of the canonical resting-state networks [69] (e.g. default-mode network, somatosensory network - Figure 3.10).

To test whether static functional connectivity was reduced in the apathetic populations, those 100 components were introduced into the dual regression pipeline. This method generates a subject specific spatial map and timecourse for all the 100 components and then runs voxelwise statistics on them.

No significant results were seen in the relevant component in both the CADASIL and sporadic SVD groups. On the lack of results with this standard method, to futher explore the functional repertoire, functional connectivity was then tested in a dynamic perspective, using LEiDA. Full results of this method can be found in Appendix A. This method extracts the leading eigenvector of the BOLD phase at all TRs (repetition times) and clusters the phase coherence signal (k-means clustering) into different PC states (functional connectivity repertoire).

In both groups, LEiDA captured a PC state that showed global incoherence – cosine similarity of -1 between all the AAL parcellations (Figure 3.11, Figure 3.12). The probability of this state occurring in apathetic and non-apathetic populations was calculated in both populations. In both the CADASIL and sporadic SVD populations, the apathetic group showed a reduced probability of entering such state. However, this difference in probabilities was significant in CADASIL ($p = 0.0356$) but not in sporadic SVD ($p = 0.317$).

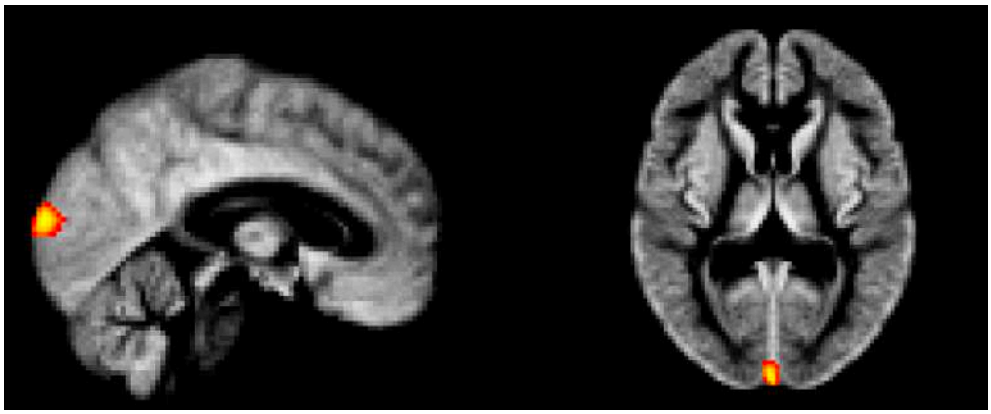

FIGURE 3.9: VBM results of CADASIL: Sagittal and transversal slices of the VBM grey matter template. P < 0.1, TFCE-corrected in red-yellow, against the study study-specific grey matter template. Apathetic CADASIL patients show significantly reduced grey matter volumes in occipital lobe areas.

From the 15 states captured using LEiDA, PC states in which the probability associated with apathy was as high or higher than the non-apathetic groups, were PC states with "weaker" connectivity – i.e. lower coherence and less regions communicating (Figure 3.13, Figure 3.14).

In both the CADASIL and sporadic SVD population, LEiDA captured a PC state associated with high coherence of regions of the occipital lobe (Figure 3.15, Figure 3.16). The probability of this state occurring in the apathetic and non-apathetic population of both cohorts was calculated in both populations. In both cohorts, the apathetic shown a significant reduced probability of entering that PC state (CADASIL: $p = 0.0448$; sporadic SVD: $p = 0.0028$).

In the CADASIL population, LEiDA captured two states with high coherence associated with the key regions linked to motivated behaviour. State 13 (Figure 3.17) shows high coherence of more internal and lower regions, including the ventromedial prefrontal cortex and the orbitofrontal cortex. State 14 (Figure 3.18) is highly coherent in higher regions of the frontal cortex. In sporadic SVD, a similar state was captured using LEiDA. State 7 (Figure 3.19) shows high coherence of nodes of the orbitofrontal cortex. The probability of these states occurring in the apathetic and non-apathetic population of both cohorts was calculated in both populations. In both cohorts, the apathetic shown a significant reduced probability of entering those PC state (CADASIL, state 13: $p = 0.0442$; CADASIL, state 14: $p = 0.0126$; sporadic SVD: $p = 0.0376$).

3.5 Computational modelling and relation to neuroimaging findings

To link back the functional connectivity measures with the behavioural findings of sensitivity to rewards and effort, the probability of occurrence of certain stages was then correlated (using

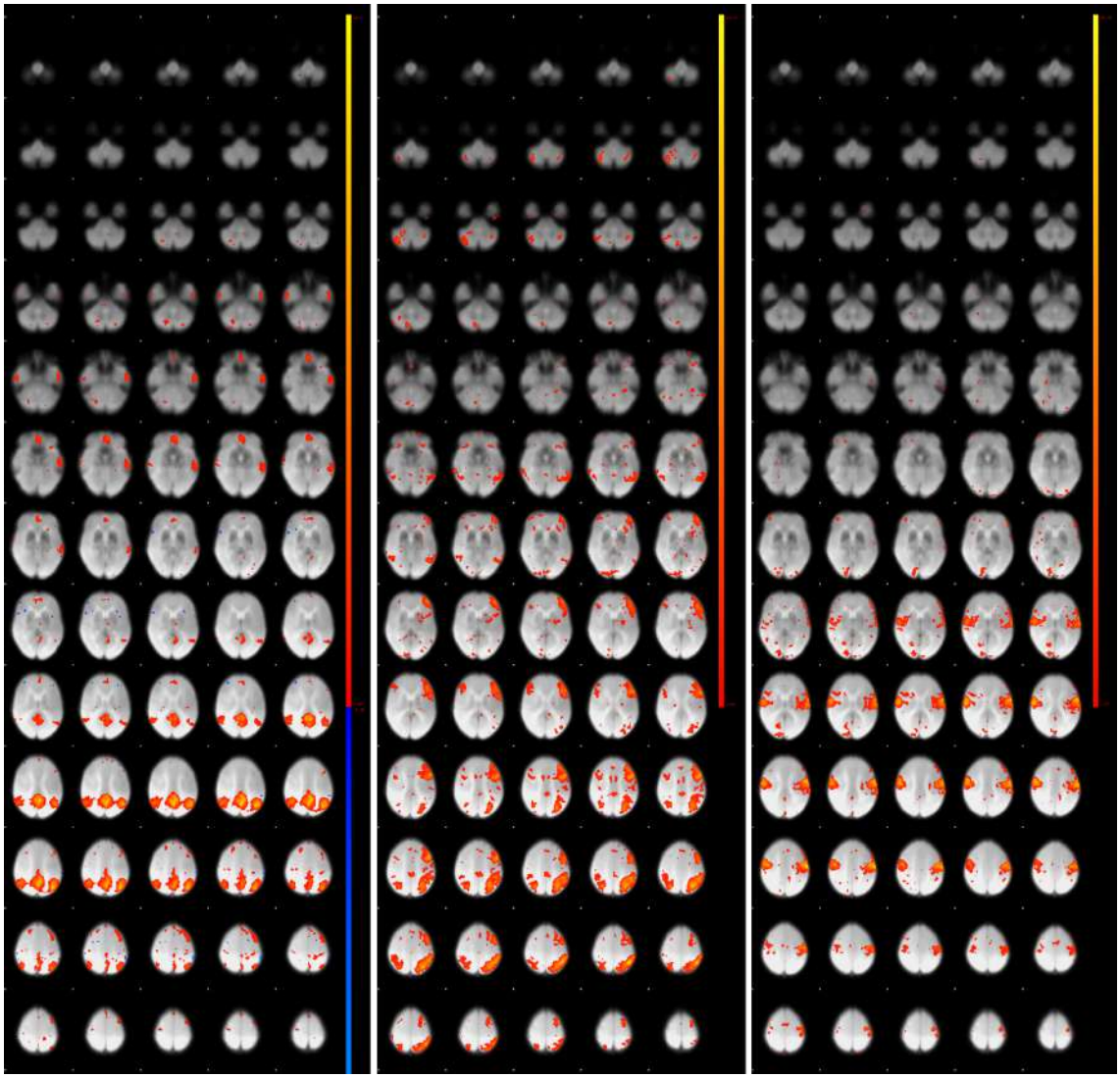

FIGURE 3.10: Example of resting-state networks captured by the ICA decomposition (left: default mode network, middle: frontotemporal network, right: somatomotor network).

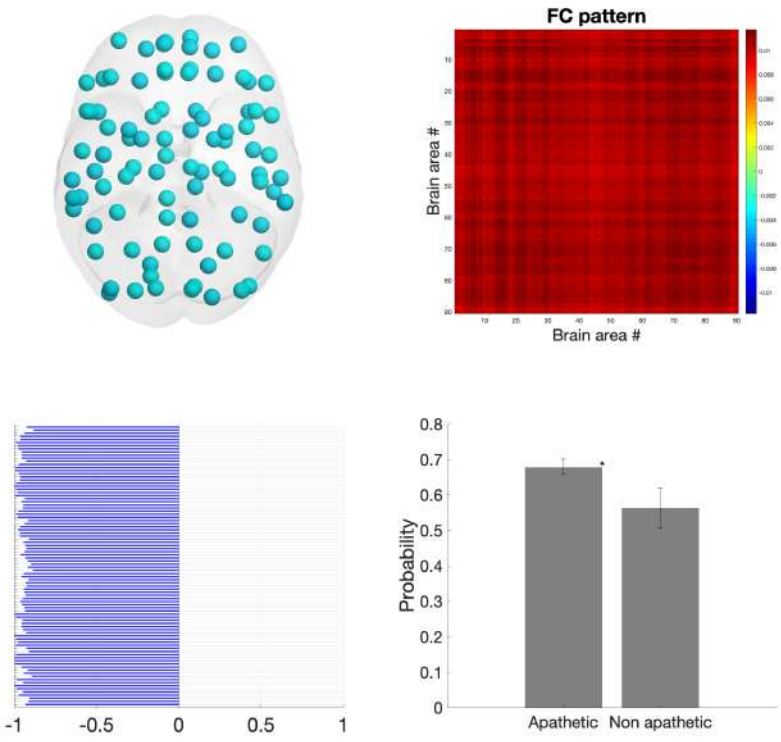

FIGURE 3.11: LEiDA in CADASIL: State 1 – global incoherence state. Top left: AAL node representation on a cortical surface, with connection strength and links; top right: Pearson correlation matrix between the 90 AAL nodes; lower left: the leading eigenvector of the phase coherence state at each brain area; lower right: difference in probability of the PC state between apathetic and non-apathetic groups, statistically tested through permutation-based t-testing.

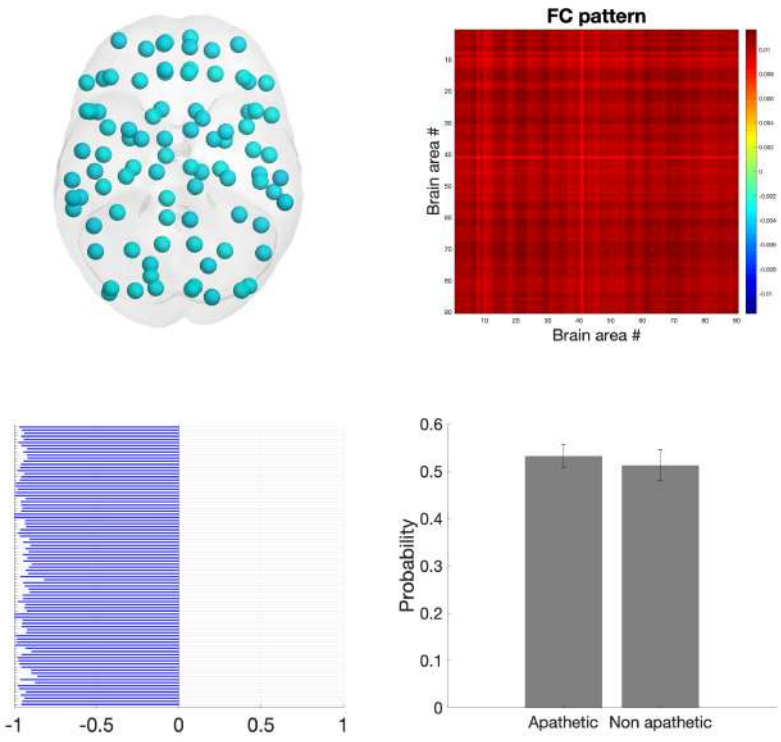

FIGURE 3.12: LEiDA in sporadic SVD: State 1 – global incoherence state. Top left: AAL node representation on a cortical surface, with connection strength and links; top right: Pearson correlation matrix between the 90 AAL nodes; lower left: the leading eigenvector of the phase coherence state at each brain area; lower right: difference in probability of the PC state between apathetic and non-apathetic groups, statistically tested through permutation-based t-testing.

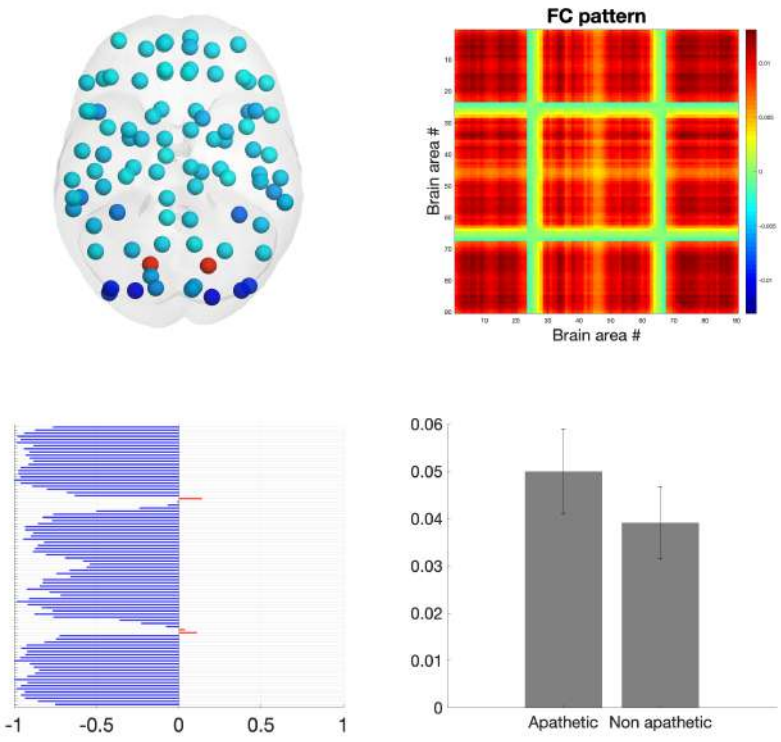

FIGURE 3.13: LEiDA in CADASIL: State 4 – weak connectivity PC state. Top left: AAL node representation on a cortical surface, with connection strength and links; top right: Pearson correlation matrix between the 90 AAL nodes; lower left: the leading eigenvector of the phase coherence state at each brain area; lower right: difference in probability of the PC state between apathetic and non-apathetic groups, statistically tested through permutation-based t-testing.

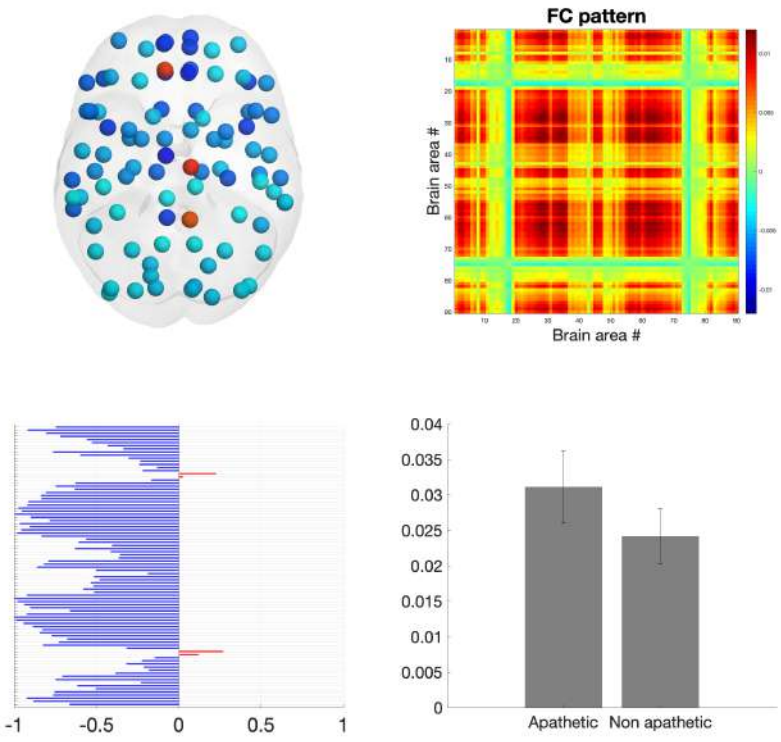

FIGURE 3.14: LEiDA in sporadic SVD: State 8 – weak connectivity PC state. Top left: AAL node representation on a cortical surface, with connection strength and links; top right: Pearson correlation matrix between the 90 AAL nodes; lower left: the leading eigenvector of the phase coherence state at each brain area; lower right: difference in probability of the PC state between apathetic and non-apathetic groups, statistically tested through permutation-based t-testing.

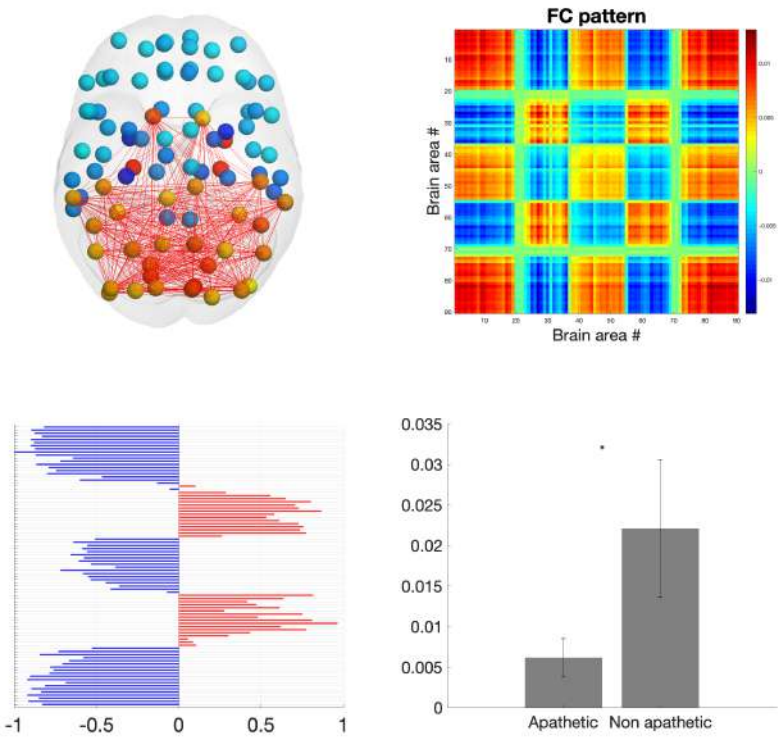

FIGURE 3.15: LEiDA in CADASIL: State 10 – occipital coherence. Top left: AAL node representation on a cortical surface, with connection strength and links; top right: Pearson correlation matrix between the 90 AAL nodes; lower left: the leading eigenvector of the phase coherence state at each brain area; lower right: difference in probability of the PC state between apathetic and non-apathetic groups, statistically tested through permutation-based t-testing.

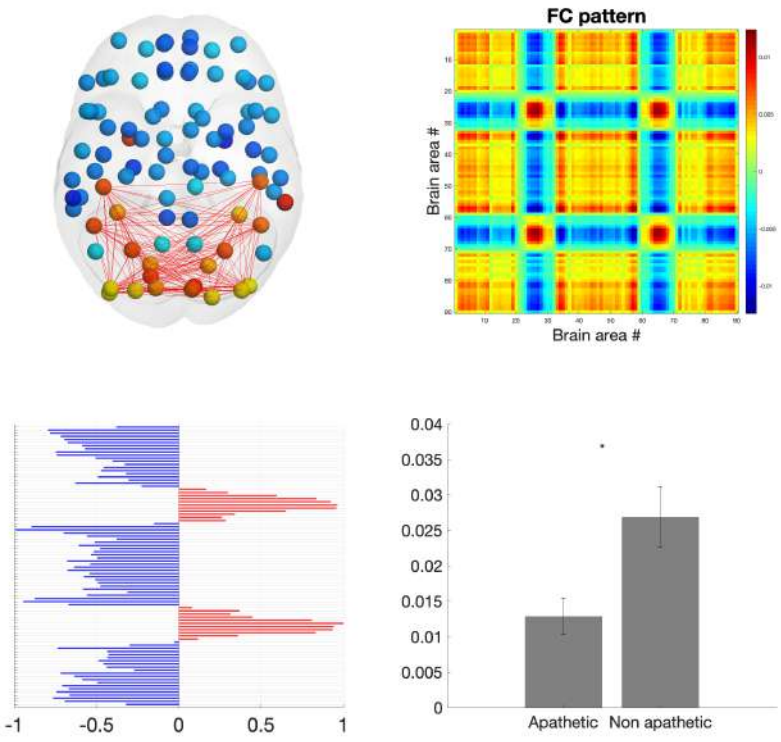

FIGURE 3.16: LEiDA in sporadic SVD: State 9 – occipital coherence. Top left: AAL node representation on a cortical surface, with connection strength and links; top right: Pearson correlation matrix between the 90 AAL nodes; lower left: the leading eigenvector of the phase coherence state at each brain area; lower right: difference in probability of the PC state between apathetic and non-apathetic groups, statistically tested through permutation-based t-testing.

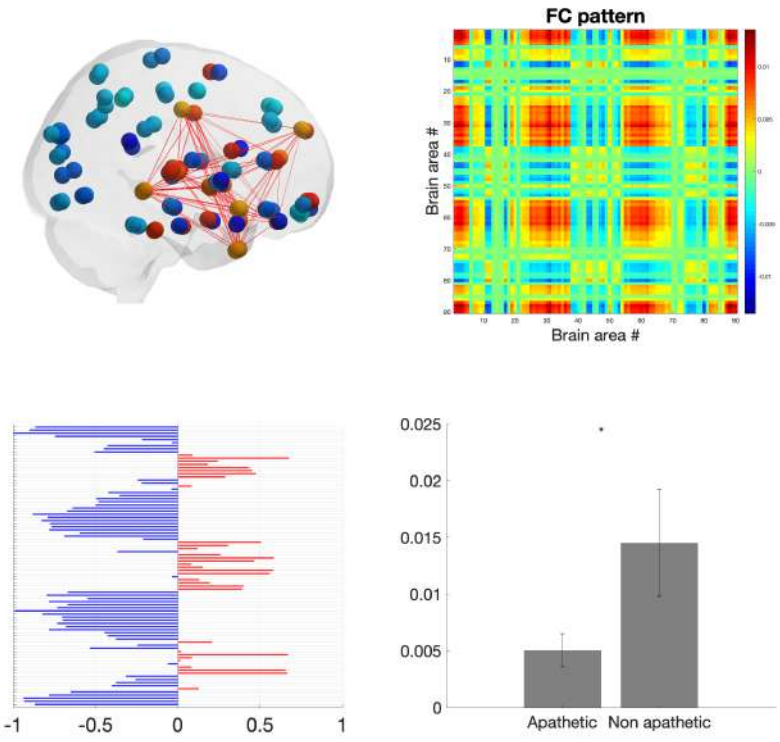

FIGURE 3.17: LEiDA in CADASIL: State 13 – prefrontal cortex coherence. Top left: AAL node representation on a cortical surface, with connection strength and links; top right: Pearson correlation matrix between the 90 AAL nodes; lower left: the leading eigenvector of the phase coherence state at each brain area; lower right: difference in probability of the PC state between apathetic and non-apathetic groups, statistically tested through permutation-based t-testing.

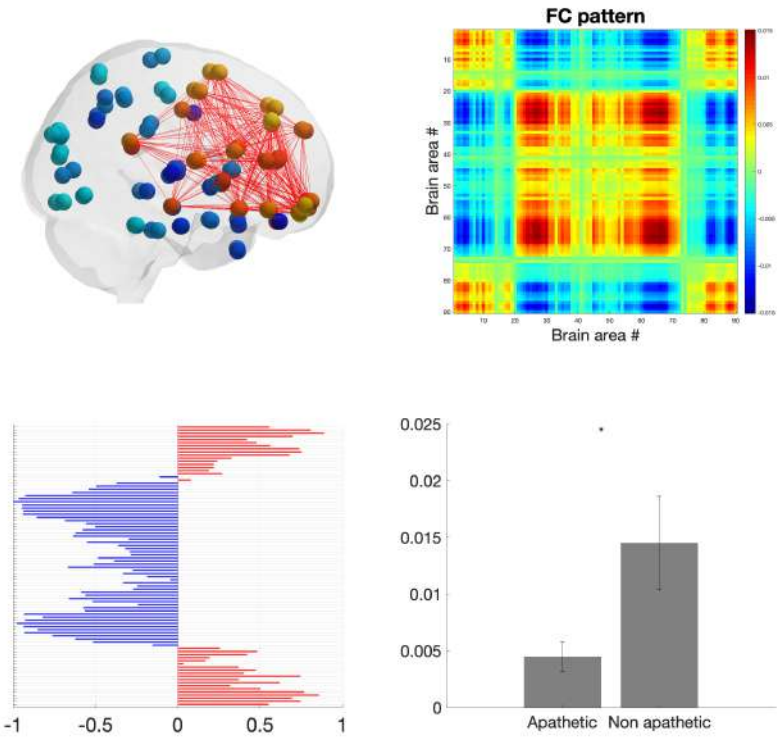

FIGURE 3.18: LEiDA in CADASIL: State 14 – prefrontal cortex coherence. Top left: AAL node representation on a cortical surface, with connection strength and links; top right: Pearson correlation matrix between the 90 AAL nodes; lower left: the leading eigenvector of the phase coherence state at each brain area; lower right: difference in probability of the PC state between apathetic and non-apathetic groups, statistically tested through permutation-based t-testing

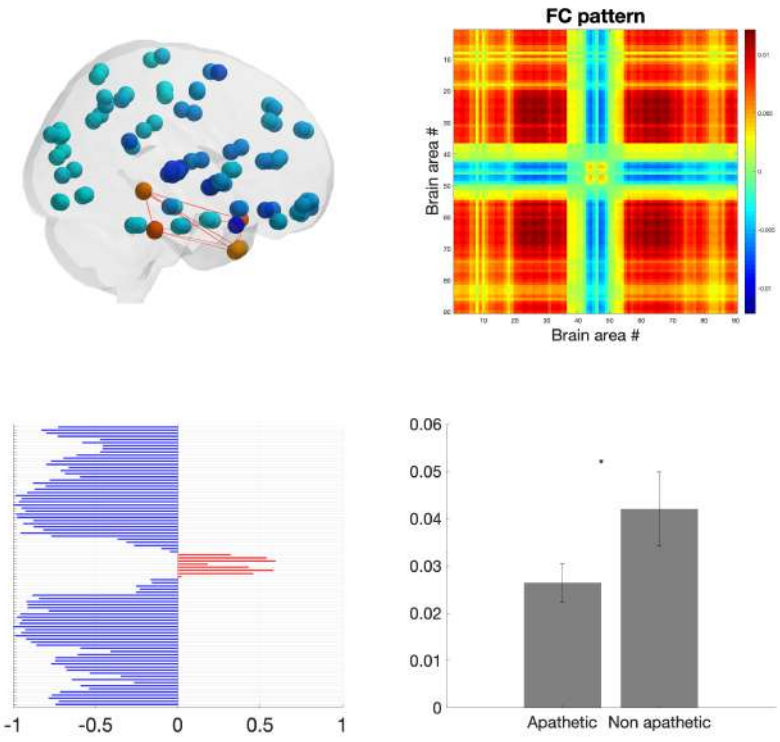

FIGURE 3.19: LEiDA in sporadic SVD: State 7 – prefrontal cortex coherence. Top left: AAL node representation on a cortical surface, with connection strength and links; top right: Pearson correlation matrix between the 90 AAL nodes; lower left: the leading eigenvector of the phase coherence state at each brain area; lower right: difference in probability of the PC state between apathetic and non-apathetic groups, statistically tested through permutation-based t-testing.

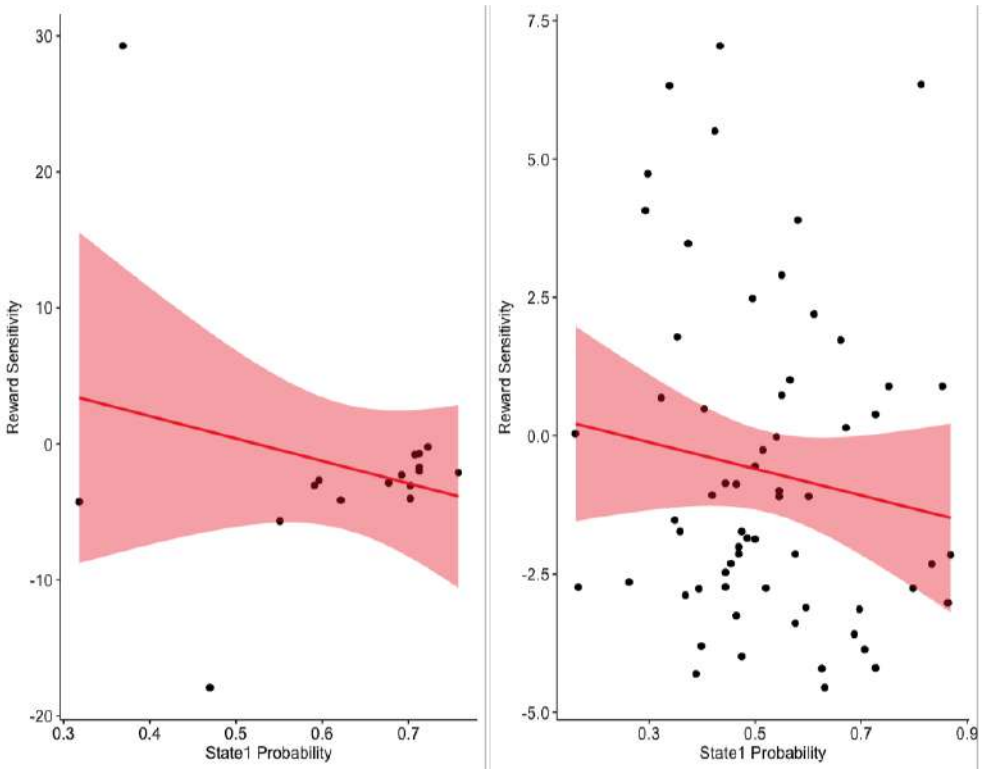

FIGURE 3.20: Plot of the Pearson correlation between the probability of occurence of the global incoherence state and the reward sensitivity estimate of each participant. On the x-axis are the state probabilities and on the y-axis the reward sensitivity parameter estimates. The orange band around the regression line is the confidence interval. Left: CADASIL, Right: sporadic SVD.

Pearson correlation) with the parameter estimates from the computational modelling. Significant difference in mean was then tested with a t-test.

We firstly looked at the correlation between reward sensitivity and the probability of occurence of the global incoherence state (Figure 3.20).

In both populations we see a very weak negative association. In neither the correlation is significant.

Secondly, we've aimed at correlating the reward sensitivity parameter estimates with the probability of occurence of occipital lobe phase coherence state (Figure 3.21).

A positive relation is seen between the state occurence probabilities and the reward sensitivity parameter estimates. This indicates an increase in connectivity of the occipital lobe is associated with an increased behavioural reward sensitivity. However, neither of the associations is statistically significant.

Lastly, we've also investigated the correlation between the reward sensitivity and the probabilities of ocurrence of the ventromedial prefrontal cortex phase coherence (Figure 3.22).

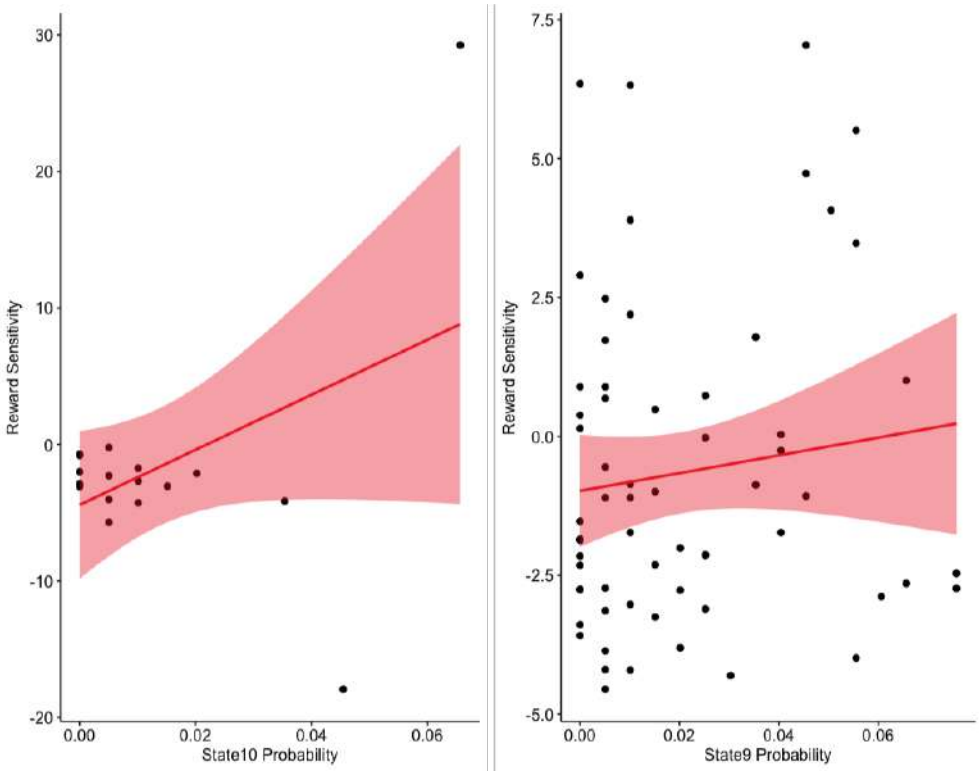

FIGURE 3.21: Plot of the Pearson correlation between the probability of occurence of the occipital phase coherence state and the reward sensitivity estimate of each participant. On the x-axis are the state probabilities and on the y-axis the reward sensitivity parameter estimates. The orange band around the regression line is the confidence interval. Left: CADASIL, Right: sporadic SVD.

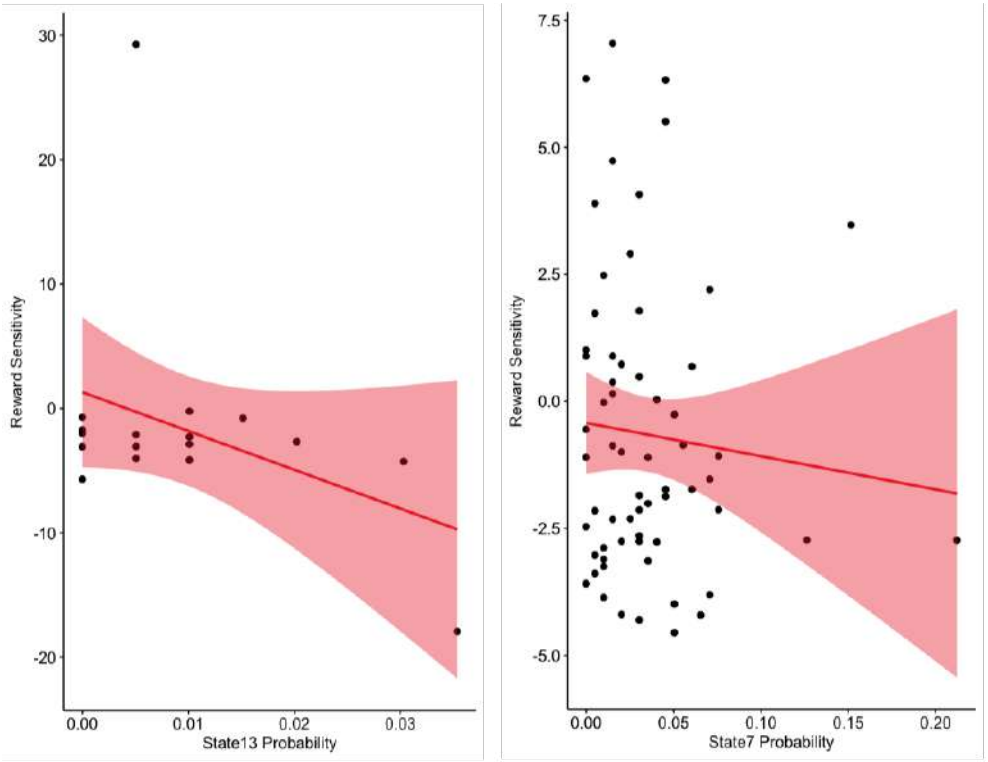

FIGURE 3.22: Plot of the Pearson correlation between the probability of occurence of the vmPFC phase coherence state and the reward sensitivity estimate of each participant. On the x-axis are the state probabilities and on the y-axis the reward sensitivity parameter estimates. The orange band around the regression line is the confidence interval. Left: CADASIL, Right: sporadic SVD.

A negative association is seen between reward sensitivity and state occurence probability. Both are not significant.

3.6 Summary of the results

From this section it's possible to understand that the apathetic group differs significantly in both populations (CADASIL and sporadic SVD) in regards to several cognitive measures. Both populations show significant reduction of quality of life and depression scores. Moreover, sporadic SVD shows significant reduction of cognitive function.

On a second approach, we've seen that apathy is associated with the reduction of white matter integrity of key regions of the corpus callosum and the anterior cingulate. This further confirms the literature. Sporadic SVD have broader damage along the corpus callosum.

Through the application of VBM it was clear that the association between apathy and grey matter degeneration is not strong. In sporadic SVD no significant results were obtained. In CADASIL, a small region of the occipital lobe has shown reduction of grey matter volume.

After evaluating the structural brain changes in association with apathy, we next assessed if the functional connectome also provided some evidence of being disrupted in association with apathy. Firstly, functional connectivity was assessed using dual regression, which considers the functional connectivity fluctuations negligible in the timeframe of the MRI scan. This method, in both populations captured canonical resting-state networks but did not show any significant reduction of functional connectivity in association with apathy.

On a second instance, functional connectivity was assessed with the novel method named LEiDA (Leading Eigenvector Dynamic Analysis). With this method we've seen that apathy is associated with higher incoherence between brain nodes and weaker connectivity (less brain nodes with reduced coactivation). Moreover, phase coherence states of key areas associated with structural changes were less probable to occur in the apathetic population when compared to non-apathetic patients.

Lastly, the reward and effort sensitivity computational modelling estimates were correlated with PC state probability, aiming at identifying a direct relation between apathetic behaviour and disrupted functional connectivity. The correlation has shown to be weak.

4 Discussion

Apathy is a syndrome of impaired motivation, which has been widely associated with reduced quality of life. From healthy human studies, the neural mechanisms and the consequent behaviour of this condition are fairly well studied. However, it's not presently clear how these systems are being disrupted in diseased populations. Apathy is a major hallmark of cerebral vascular disease, which is a major contributor to vascular dementia. Based on previous literature of apathy, this project aimed at studying changes of brain structure and function and to understand their relation to each other and to computational modelling estimates of apathetic behaviour. It's possible to see this study as a first step to answering the question of whether apathy is a good biomarker for the progression to vascular dementia in cerebral small vessel disease populations.

From the results section it's possible to see that the populations at hand differed significantly in regard to depression scores and self-reported quality of life. In a general understanding, both things seem very closely related and it's our hypothesis that depression is partially the outcome of this reduction in motivated behaviour, which leads to reduced quality of life.

Moreover, the sporadic SVD group differed significantly in measures of cognitive function. This might be related to the patients' more advanced age when compared to the CADASIL group.

All in all, these differences also mean that to better isolate the effects on apathy in the imaging results, the data inputted could have been controlled then for cognitive function and depression. The lack of this control could be skewing the results in some unexpected ways.

Following, both populations' apathetic group show an evident difference in performance on the effort-based decision-making task. Both apathetic groups accepted, in general, fewer offers than their non-apathetic counterparts, indicating a disruption of self-initiated motivated behaviour. The difference in sporadic SVD patients was smaller when compared to the CADASIL population. This might be due to the other brain changes (related to age) also influencing behaviour.

Interestingly, the biggest difference in accepted offers seen between the apathetic and non-apathetic populations were seen in low reward areas of the task's decision space, regardless of the effort required. This indicates this loss of reward sensitivity in apathetic patients.

Next, to study the neural mechanisms of apathy and how they relate to the above estimates, we firstly started by looking at brain anatomy. TBSS identified, in both cerebral SVD, the regions where fractional anisotropy was significantly associated with apathy. The common denominator of both groups was the reduction of fractional anisotropy within the tracts of the body of the corpus callosum and the anterior cingulate. These findings are consistent with previous literature of motivated behaviour as the anterior cingulum is closely associated with the anterior cingulate cortex. These tracts link the amygdala and regions which include the ventral striatum and the vmPFC. Additionally, in CADASIL (and not in sporadic SVD), reduced white matter integrity of the splenium of the corpus callosum was identified. This finding is not explained by the current literature but might have value in further understanding the effects of apathy in this group. Moreover, sporadic SVD shows reduced white matter integrity more widely than the CADASIL group. This can be explained by the extra comorbidities that this older cohort might have.

No association between the fractional anisotropy values and the white matter hyperintensity load of each subject was found, indicating further that WMH do not necessarily contribute to apathetic behaviour.

Continuing looking at brain anatomy, we were interested in identifying which areas of the brain show reduced grey matter volume in association with apathy and if these had any relation to areas of reduced white matter integrity. Voxel-based morphometry analysis shown no significant reduction of grey matter in the sporadic SVD group. It showed significance in the CADASIL in areas of the occipital lobe. This effect could be driven either by the reduction of white matter integrity of the splenium of the corpus callosum or by not controlling perfusion in our GLM. Different areas of the brain have different degrees of perfusion. This results in having certain voxels being more intense regardless of the type of tissue present. This would lead to a false-positive finding of the VBM analysis. In the absence of literature, pointing towards a logical interpretation of this grey matter volume change being associated with apathy, we believe that this change might be caused by the latter explanation. However, further work should be done to confirm this idea. The second imaging approach aimed at looking at functional changes of the brain in association with apathy. The first interesting finding of LEiDA is related to the global incoherence state it captures in both the CADASIL and sporadic SVD populations. The existence of this state points to an idea in which functional connectivity is composed of slow transitions between discrete PC states. Apathetic individuals spend more time in this incoherent state than their non-apathetic counterparts. This might indicate one of two things: either disrupted motivation is reducing the rate of transition in apathy patients or it's making it totally impossible for those to have access to certain states. Further investigation needs to happen to understand the switching mechanisms of functional connectivity. A non-significant result in the sporadic SVD population can be explained by how heterogenous that population is (in terms of other associated pathologies, or in apathetic behaviour). From all the 15 states that LEiDA captured, the ones that show a similar probability of occurring in both the apathetic and non-apathetic groups were all states of "weak" connectivity. This finding might indicate that

the ability of apathy patients entering "higher order" states is impaired. It's not clear if these "weaker" states represent a lower cognitive process nor if a "higher order" state requires more neural resources to be explored. However, studying the difference between high order and low order functional states might be useful to further explore the impairment seen in apathy. LEiDA captured a PC state with high coherence of the occipital lobe. The difference in probability of the apathetic and non-apathetic group is significant in both SVD populations. This is an interesting result for two reasons: firstly, there's no literature on the importance of the occipital lobe for motivated behaviour; secondly, there's no structural changes in sporadic SVD that indicate this disruption in functional connectivity. Changes in grey matter in CADASIL can be explained by lack of control for perfusion, however, white matter integrity in the splenium of the corpus callosum might indicate otherwise. A more focused, region analysis of the occipital lobe needs to be done to disentangle what can be the source of this disruption. LEiDA captured in both cerebral SVD populations states whose coherence overlaps with regions of the prefrontal and orbifrontal cortex. This would be coherent with the VBM findings, where reduced grey matter volume was identified in similar regions. However, this grey matter effect was not seen in the sporadic SVD group. This might indicate that functional connectivity is picking changes in the absence of structural changes. In literature it's assumed that damage to grey or white matter are the root of damage to the functional connectome. However, such results might indicate that this order is more complex and that both affect one another in both directions. One explanation for this finding is that disruption in functional connectivity, due to some particular reason, is causing grey matter volume. This had happened to CADASIL patients but not to the sporadic SVD ones. More information about this mechanism could be obtained if age of onset of this apathetic behaviour was considered.

To tie down the functional connectivity findings and tying them down with their behavioural underpinnings, the computational modelling parameter estimates of reward sensitivity were correlated with the probabililty of occurence of the key disrupted phase coherence states derived from LEiDA. Contrary to our hypothesis, these didn't associate strongly. This might be due to the courseness of phase coherence states extracted. If more parcellations were to be used, the exact regions of disrupted functional connectivity could be assessed and the likely the asssociation with the behaviour parameters would have been stronger.

4.1 Study limitations

One major limitation of this study arises from the neuroimaging protocol used. On one hand due to the lack of spatial resolution of the resting state functional MRI sequences - increasing the resolution of the scan would result in increasing the time of scanning, and making the data acquisition more impractical, higher resolution would allow the imaging algorithms to better determine resting-state networks. Moreover, the lack of field-maps made more difficult the denoising of the data. On the other hand, the diffusion data was comprised of only 32 directions.

Having a dataset with 60 or more diffusion directions would allow for a more detailed and trustworthy TBSS analysis. Secondly, the parcellation scheme used for the dynamical analysis of the resting state data is probably too coarse for this kind of analysis. The results would benefit for a finer atlas, that wasn't structurally defined. Thirdly, the CADASIL study power was also influenced by the small number of patients. Its importance is linked to being a pure model of vascular dementia, that could be used to better explain the mechanisms of the disorder. However, small numbers result in noisier results and a lower statistical power. Also, the heterogeneity of the sporadic SVD population hindered the possible conclusions of the study. Lastly, the lack of existent literature on dynamic functional connectivity and its relation to disease only allowed some of our conclusion to be mere speculation.

4.2 Future work

During the course of this project, a lot of ideas arose to make the study more robust and the findings more significant. However, either due to time or technical constraints, not all the ideas were implemented.

In order to make the results more robust one could control the models applied in the study for depression, cognitive function and measures of perfusion.

To have a better understanding how apathy develops with development of disease, we could have done similar analysis but also splitting the populations based on the severity of the vascular pathology. Moreover, splitting the apathetic population in regard to the severity of their apathy and age at onset could also have been informative.

One of the shortcomings of MRI is its lack of temporal resolution. For a finer understanding of the dynamical repertoire of functional connectivity, applying LEiDA to a higher temporal resolution dataset (e.g. EEG/MEG) could prove insightful.

5 Conclusions

All in all, this study represents a first step towards understanding the biomarker potential of apathy, here associated with an impaired goal-directed behaviour, in cerebral small vessel disease. This project comprises a comprehensive neural study of apathy and its mechanisms. Following previous work, we make the case that apathy in cerebral small vessel disease is firstly associated with reduction of fractional anisotropy in key tracts. We also show that this reduction of white matter integrity is associated with reduction of grey matter volume and disrupted functional connectivity. There has been a growing body of science interested in the understanding of the brain function through the analysis of BOLD fluctuation and how the information inferred from it surpasses the simple analysis of structural changes. Here, we've shown that apathetic patients show "weaker" and more incoherent overall repertoire of functional states when compared to their non-apathetic counterparts. Apathetic patients also show reduced probability of occurrence of phase coherence states of regions of importance to the motivated behaviour circuitry. // Moreover, our results suggest, through the association between the PC states and the parameter estimates of reward and effort sensitivity, the lack of existence of a functionally connected motivation network. However, finer functional connectivity parcellation and a bigger sample size are needed to provide more insight on this relationship.

The overall results shine a light into the understanding of the neural dynamics of apathy in cerebral small vessel disease. Nevertheless, future longitudinal research is needed to test the relevance of apathy as a predictor of vascular dementia in cerebral small vessel disease. It is also in our opinion that future research could push towards using a higher temporal resolution method (like EEG) to measure the repertoire of functional connectivity.

Bibliography

[1] K. Bayles, K. McCullough, and C. Tomoeda, *Cognitive-Communication Disorders of Dementia : Definition, Diagnosis, and Treatment, Third Edition.* Plural Publishing, Incorporated, 2018, p. 282, ISBN: 1635500591.

[2] A. F. Jorm and D. Jolley, "The incidence of dementia: a meta-analysis", *Neurology*, vol. 51, no. 3, pp. 728–733, 1998, ISSN: 0028-3878.

[3] L. Fratiglioni, D. De Ronchi, and H. Ag??ero Torres, "Worldwide prevalence and incidence of dementia", *Drugs & Aging*, vol. 15, no. 5, pp. 365–375, 1999, ISSN: 1170-229X.

[4] W. M. van der Flier and P Scheltens, "Epidemiology and risk factors of dementia.", *Journal of neurology, neurosurgery, and psychiatry*, vol. 76 Suppl 5, no. suppl 5, pp. v2–7, 2005, ISSN: 0022-3050.

[5] J. T. O'Brien, T. Erkinjuntti, B. Reisberg, G. Roman, T. Sawada, L. Pantoni, J. V. Bowler, C. Ballard, C. DeCarli, P. B. Gorelick, K. Rockwood, A. Burns, S. Gauthier, and S. T. DeKosky, "Vascular cognitive impairment", *The Lancet Neurology*, vol. 2, no. 2, pp. 89–98, 2003, ISSN: 1474-4422.

[6] G. T. Stebbins, D. L. Nyenhuis, C. Wang, J. L. Cox, S. Freels, K. Bangen, L. DeToledo-Morrell, K. Sripathirathan, M. Moseley, D. A. Turner, J. D. E. Gabrieli, and P. B. Gorelick, "Gray matter atrophy in patients with ischemic stroke with cognitive impairment.", *Stroke*, vol. 39, no. 3, pp. 785–93, 2008, ISSN: 1524-4628.

[7] A.-J. Zhang, X.-J. Yu, and M. Wang, "The clinical manifestations and pathophysiology of cerebral small vessel disease", *Neuroscience Bulletin*, vol. 26, no. 3, pp. 257–264, 2010, ISSN: 1673-7067.

[8] S. E. Vermeer, W. T. Longstreth, and P. J. Koudstaal, "Silent brain infarcts: a systematic review", *The Lancet Neurology*, vol. 6, no. 7, pp. 611–619, 2007, ISSN: 1474-4422.

[9] N. S. Rost, R. M. Rahman, A Biffi, E. E. Smith, A Kanakis, K Fitzpatrick, F Lima, B. B. Worrall, J. F. Meschia, R. D. Brown, T. G. Brott, A. G. Sorensen, S. M. Greenberg, K. L. Furie, and J Rosand, "White matter hyperintensity volume is increased in small vessel stroke subtypes.", *Neurology*, vol. 75, no. 19, pp. 1670–7, 2010, ISSN: 1526-632X.

[10] F. N. Doubal, A. M. J. MacLullich, K. J. Ferguson, M. S. Dennis, and J. M. Wardlaw, "Enlarged perivascular spaces on mri are a feature of cerebral small vessel disease.", *Stroke*, vol. 41, no. 3, pp. 450–4, 2010, ISSN: 1524-4628.

[11] C. Cordonnier, R. Al-Shahi Salman, and J. Wardlaw, "Spontaneous brain microbleeds: systematic review, subgroup analyses and standards for study design and reporting", *Brain*, vol. 130, no. 8, pp. 1988–2003, 2007, ISSN: 0006-8950.

[12] B. S. Aribisala, M. C. Valdés Hernández, N. A. Royle, Z. Morris, S. Muñoz Maniega, M. E. Bastin, I. J. Deary, and J. M. Wardlaw, "Brain atrophy associations with white matter lesions in the ageing brain: the lothian birth cohort 1936", *European Radiology*, vol. 23, no. 4, pp. 1084–1092, 2013, ISSN: 0938-7994.

[13] M. O'Sullivan, "Imaging small vessel disease: lesion topography, networks, and cognitive deficits investigated with mri.", *Stroke*, vol. 41, no. 10 Suppl, S154–8, 2010, ISSN: 1524-4628.

[14] S. Reyes, A. Viswanathan, O. Godin, C. Dufouil, S. Benisty, K. Hernandez, A. Kurtz, E. Jouvent, M. O'Sullivan, V. Czernecki, M. G. Bousser, M. Dichgans, and H. Chabriat, "Apathy", *Neurology*, vol. 72, no. 10, pp. 905–910, 2009, ISSN: 0028-3878.

[15] J. Tay, A. M. Tuladhar, M. J. Hollocks, R. L. Brookes, D. J. Tozer, T. R. Barrick, M. Husain, F.-E. de Leeuw, and H. S. Markus, "Apathy is associated with large-scale white matter network disruption in small vessel disease.", *Neurology*, vol. 92, no. 11, e1157–e1167, 2019, ISSN: 1526-632X.

[16] J. M. Wardlaw, C. Smith, and M. Dichgans, "Mechanisms of sporadic cerebral small vessel disease: insights from neuroimaging", *The Lancet Neurology*, vol. 12, no. 5, pp. 483–497, 2013, ISSN: 1474-4422.

[17] R. S. Marin, "Apathy: a neuropsychiatric syndrome", *The Journal of Neuropsychiatry and Clinical Neurosciences*, vol. 3, no. 3, pp. 243–254, 1991, ISSN: 0895-0172.

[18] C. A. Yeager and L. Hyer, "Apathy in dementia: relations with depression, functional competence, and quality of life", *Psychological Reports*, vol. 102, no. 3, pp. 718–722, 2008, ISSN: 0033-2941.

[19] C. Tiel, F. K. Sudo, G. S. Alves, L. Ericeira-Valente, D. M. Moreira, J. Laks, and E. Engelhardt, "Neuropsychiatric symptoms in vascular cognitive impairment: a systematic review.", *Dementia & neuropsychologia*, vol. 9, no. 3, pp. 230–236, 2015, ISSN: 1980-5764.

[20] C. Le Heron, M. Apps., and M. Husain, "The anatomy of apathy: a neurocognitive framework for amotivated behaviour", *Neuropsychologia*, vol. 118, pp. 54–67, 2018, ISSN: 0028-3932.

[21] S. N. Haber and T. E. Behrens, "The neural network underlying incentive-based learning: implications for interpreting circuit disruptions in psychiatric disorders", *Neuron*, vol. 83, no. 5, pp. 1019–1039, 2014, ISSN: 0896-6273.

[22] W Schultz, P Dayan, P. R. Montague, R. Deichmann, K. Friston, and R. J. Dolan, "A neural substrate of prediction and reward.", *Science (New York, N.Y.)*, vol. 275, no. 5306, pp. 1593–9, 1997, ISSN: 0036-8075.

[23] C. Padoa-Schioppa, "Neurobiology of economic choice: a good-based model", *Annual Review of Neuroscience*, vol. 34, no. 1, pp. 333–359, 2011, ISSN: 0147-006X.

[24] E. J. Nunes, P. A. Randall, S. Podurgiel, M. Correa, and J. D. Salamone, "Nucleus accumbens neurotransmission and effort-related choice behavior in food motivation: effects of drugs acting on dopamine, adenosine, and muscarinic acetylcholine receptors", *Neuroscience & Biobehavioral Reviews*, vol. 37, no. 9, pp. 2015–2025, 2013, ISSN: 0149-7634.

[25] C. Le Heron, C. B. Holroyd, J. Salamone, and M. Husain, "Brain mechanisms underlying apathy.", *Journal of neurology, neurosurgery, and psychiatry*, vol. 90, no. 3, pp. 302–312, 2019, ISSN: 1468-330X.

[26] P.-H. Yeh, K. Simpson, T. C. Durazzo, S. Gazdzinski, and D. J. Meyerhoff, "Tract-based spatial statistics (tbss) of diffusion tensor imaging data in alcohol dependence: abnormalities of the motivational neurocircuitry.", *Psychiatry research*, vol. 173, no. 1, pp. 22–30, 2009, ISSN: 0165-1781.

[27] T. Behrens, H. J. Berg, S. Jbabdi, M. Rushworth, and M. Woolrich, "Probabilistic diffusion tractography with multiple fibre orientations: what can we gain?", *NeuroImage*, vol. 34, no. 1, pp. 144–155, 2007, ISSN: 10538119.

[28] O. Sporns, G. Tononi, and R. Kötter, "The human connectome: a structural description of the human brain", *PLoS Computational Biology*, vol. 1, no. 4, e42, 2005, ISSN: 1553-734X.

[29] B. Biswal, F. Zerrin Yetkin, V. M. Haughton, and J. S. Hyde, "Functional connectivity in the motor cortex of resting human brain using echo-planar mri", *Magnetic Resonance in Medicine*, vol. 34, no. 4, pp. 537–541, 1995, ISSN: 07403194.

[30] C. Chang and G. H. Glover, "Time–frequency dynamics of resting-state brain connectivity measured with fmri", *NeuroImage*, vol. 50, no. 1, pp. 81–98, 2010, ISSN: 10538119.

[31] S. M. Smith, T. E. Nichols, D. Vidaurre, A. M. Winkler, T. E. J. Behrens, M. F. Glasser, K. Ugurbil, D. M. Barch, D. C. Van Essen, and K. L. Miller, "A positive-negative mode of population covariation links brain connectivity, demographics and behavior", *Nature Neuroscience*, vol. 18, no. 11, pp. 1565–1567, 2015, ISSN: 1097-6256.

[32] M. J. Hollocks, A. J. Lawrence, R. L. Brookes, T. R. Barrick, R. G. Morris, M. Husain, and H. S. Markus, "Differential relationships between apathy and depression with white matter microstructural changes and functional outcomes", *Brain*, vol. 138, no. 12, pp. 3803–3815, 2015, ISSN: 0006-8950.

[33] J. Tay, A. M. Tuladhar, M. J. Hollocks, R. L. Brookes, D. J. Tozer, T. R. Barrick, M. Husain, F.-E. de Leeuw, and H. S. Markus, "Apathy is associated with large-scale white matter network disruption in small vessel disease", *Neurology*, vol. 92, no. 11, 10.1212/WNL.0000000000007095, 2019, ISSN: 0028-3878.

[34] E Jouvent, S Reyes, J.-F. Mangin, P Roca, M Perrot, B Thyreau, D Hervé, M Dichgans, and H Chabriat, "Apathy is related to cortex morphology in cadasil. a sulcal-based morphometry study.", *Neurology*, vol. 76, no. 17, pp. 1472–7, 2011, ISSN: 1526-632X.

[35] P. Kochunov, P. M. Thompson, T. R. Coyle, J. L. Lancaster, V. Kochunov, D. Royall, J.-F. Mangin, D. Rivière, and P. T. Fox, "Relationship among neuroimaging indices of cerebral health during normal aging", *Human Brain Mapping*, vol. 29, no. 1, pp. 36–45, 2008, ISSN: 10659471.

[36] E. R. Sowell, B. S. Peterson, P. M. Thompson, S. E. Welcome, A. L. Henkenius, and A. W. Toga, "Mapping cortical change across the human life span", *Nature Neuroscience*, vol. 6, no. 3, pp. 309–315, 2003, ISSN: 1097-6256.

[37] O. Querbes, F. Aubry, J. Pariente, J.-A. Lotterie, J.-F. Démonet, V. Duret, M. Puel, I. Berry, J.-C. Fort, and P. Celsis, "Early diagnosis of alzheimer's disease using cortical

thickness: impact of cognitive reserve", *Brain*, vol. 132, no. 8, pp. 2036–2047, 2009, ISSN: 1460-2156.

[38] L. M. Rimol, R. Nesvåg, D. J. Hagler, Ø. Bergmann, C. Fennema-Notestine, C. B. Hartberg, U. K. Haukvik, E. Lange, C. J. Pung, A. Server, I. Melle, O. A. Andreassen, I. Agartz, and A. M. Dale, "Cortical volume, surface area, and thickness in schizophrenia and bipolar disorder", *Biological Psychiatry*, vol. 71, no. 6, pp. 552–560, 2012, ISSN: 0006-3223.

[39] J. Su, M. Wang, S. Ban, L. Wang, X. Cheng, F. Hua, Y. Tang, H. Zhou, Y. Zhai, X. Du, and J. Liu, "Relationship between changes in resting-state spontaneous brain activity and cognitive impairment in patients with cadasil", *The Journal of Headache and Pain*, vol. 20, no. 1, p. 36, 2019, ISSN: 1129-2369.

[40] G. S. Alexopoulos, M. J. Hoptman, G. Yuen, D. Kanellopoulos, J. K. Seirup, K. O. Lim, and F. M. Gunning, "Functional connectivity in apathy of late-life depression: a preliminary study", *Journal of Affective Disorders*, vol. 149, no. 1-3, pp. 398–405, 2013, ISSN: 0165-0327.

[41] H. C. Baggio, B. Segura, J. L. Garrido-Millan, M.-J. Marti, Y. Compta, F. Valldeoriola, E. Tolosa, and C. Junque, "Resting-state frontostriatal functional connectivity in parkinson's disease-related apathy", *Movement Disorders*, vol. 30, no. 5, pp. 671–679, 2015, ISSN: 08853185.

[42] R. S. Marin, R. C. Biedrzycki, and S Firinciogullari, "Reliability and validity of the apathy evaluation scale.", *Psychiatry research*, vol. 38, no. 2, pp. 143–62, 1991, ISSN: 0165-1781.

[43] P Sockeel, K Dujardin, D Devos, C Denève, A Destée, and L Defebvre, "The lille apathy rating scale (lars), a new instrument for detecting and quantifying apathy: validation in parkinson's disease.", *Journal of neurology, neurosurgery, and psychiatry*, vol. 77, no. 5, pp. 579–84, 2006, ISSN: 0022-3050.

[44] A. T. Beck, R. A. Steer, and M. G. Carbin, "Psychometric properties of the beck depression inventory: twenty-five years of evaluation", *Clinical Psychology Review*, vol. 8, no. 1, pp. 77–100, 1988, ISSN: 0272-7358.

[45] J. A. Yesavage and J. I. Sheikh, "9/geriatric depression scale (gds)", *Clinical Gerontologist*, vol. 5, no. 1-2, pp. 165–173, 1986, ISSN: 0731-7115.

[46] S. Crawford, L. Whitnall, J. Robertson, and J. J. Evans, "A systematic review of the accuracy and clinical utility of the addenbrooke's cognitive examination and the addenbrooke's cognitive examination-revised in the diagnosis of dementia", *International Journal of Geriatric Psychiatry*, vol. 27, no. 7, pp. 659–669, 2012, ISSN: 08856230.

[47] C. W. Topp, S. D. Østergaard, S. Søndergaard, and P. Bech, "The who-5 well-being index: a systematic review of the literature", *Psychotherapy and Psychosomatics*, vol. 84, no. 3, pp. 167–176, 2015, ISSN: 0033-3190.

[48] K. J. Gorgolewski, T. Auer, V. D. Calhoun, R. C. Craddock, S. Das, E. P. Duff, G. Flandin, S. S. Ghosh, T. Glatard, Y. O. Halchenko, D. A. Handwerker, M. Hanke, D. Keator, X. Li, Z. Michael, C. Maumet, B. N. Nichols, T. E. Nichols, J. Pellman, J.-B. Poline, A. Rokem, G. Schaefer, V. Sochat, W. Triplett, J. A. Turner, G. Varoquaux, and R. A. Poldrack, "The brain imaging data structure, a format for organizing and describing

outputs of neuroimaging experiments", *Scientific Data*, vol. 3, no. 1, p. 160 044, 2016, ISSN: 2052-4463.

[49] S. M. Smith, "Fast robust automated brain extraction", *Human Brain Mapping*, vol. 17, no. 3, pp. 143–155, 2002, ISSN: 1065-9471.

[50] J. Juntu, J. Sijbers, D. Dyck, and J. Gielen, "Bias field correction for mri images", in, Springer, Berlin, Heidelberg, 2005, pp. 543–551.

[51] Y. Zhang, M. Brady, and S. Smith, "Segmentation of brain mr images through a hidden markov random field model and the expectation-maximization algorithm", *IEEE Transactions on Medical Imaging*, vol. 20, no. 1, pp. 45–57, 2001, ISSN: 02780062.

[52] J. L. Andersson, S. Skare, and J. Ashburner, "How to correct susceptibility distortions in spin-echo echo-planar images: application to diffusion tensor imaging", *NeuroImage*, vol. 20, no. 2, pp. 870–888, 2003, ISSN: 10538119.

[53] S. M. Smith, M. Jenkinson, M. W. Woolrich, C. F. Beckmann, T. E. Behrens, H. Johansen-Berg, P. R. Bannister, M. De Luca, I. Drobnjak, D. E. Flitney, R. K. Niazy, J. Saunders, J. Vickers, Y. Zhang, N. De Stefano, J. M. Brady, and P. M. Matthews, "Advances in functional and structural mr image analysis and implementation as fsl", *NeuroImage*, vol. 23, S208–S219, 2004, ISSN: 10538119.

[54] J. L. Andersson and S. N. Sotiropoulos, "An integrated approach to correction for off-resonance effects and subject movement in diffusion mr imaging", *NeuroImage*, vol. 125, pp. 1063–1078, 2016, ISSN: 10538119.

[55] M. Jenkinson, P. Bannister, M. Brady, and S. Smith, "Improved optimization for the robust and accurate linear registration and motion correction of brain images.", *NeuroImage*, vol. 17, no. 2, pp. 825–41, 2002, ISSN: 1053-8119.

[56] L. Griffanti, G. Zamboni, A. Khan, L. Li, G. Bonifacio, V. Sundaresan, U. G. Schulz, W. Kuker, M. Battaglini, P. M. Rothwell, and M. Jenkinson, "Bianca (brain intensity abnormality classification algorithm): a new tool for automated segmentation of white matter hyperintensities", *NeuroImage*, vol. 141, pp. 191–205, 2016, ISSN: 1053-8119.

[57] M. Kubicki, H. Park, C. Westin, P. Nestor, R. Mulkern, S. Maier, M. Niznikiewicz, E. Connor, J. Levitt, M. Frumin, R. Kikinis, F. Jolesz, R. McCarley, and M. Shenton, "Dti and mtr abnormalities in schizophrenia: analysis of white matter integrity", *NeuroImage*, vol. 26, no. 4, pp. 1109–1118, 2005, ISSN: 1053-8119.

[58] L. S. Hamilton, J. G. Levitt, J. O'Neill, J. R. Alger, E. Luders, O. R. Phillips, R. Caplan, A. W. Toga, J. McCracken, and K. L. Narr, "Reduced white matter integrity in attention-deficit hyperactivity disorder", *Neuroreport*, vol. 19, no. 17, p. 1705, 2008.

[59] S. M. Smith, M. Jenkinson, H. Johansen-Berg, D. Rueckert, T. E. Nichols, C. E. Mackay, K. E. Watkins, O. Ciccarelli, M. Z. Cader, P. M. Matthews, and T. E. Behrens, "Tract-based spatial statistics: voxelwise analysis of multi-subject diffusion data", *NeuroImage*, vol. 31, no. 4, pp. 1487–1505, 2006, ISSN: 10538119.

[60] S SMITH and T NICHOLS, "Threshold-free cluster enhancement: addressing problems of smoothing, threshold dependence and localisation in cluster inference", *NeuroImage*, vol. 44, no. 1, pp. 83–98, 2009, ISSN: 10538119.

[61] A. M. Winkler, G. R. Ridgway, M. A. Webster, S. M. Smith, and T. E. Nichols, "Permutation inference for the general linear model", *NeuroImage*, vol. 92, pp. 381–397, 2014, ISSN: 1053-8119.

[62] G. Douaud, S. Smith, M. Jenkinson, T. Behrens, H. Johansen-Berg, J. Vickers, S. James, N. Voets, K. Watkins, P. M. Matthews, and A. James, "Anatomically related grey and white matter abnormalities in adolescent-onset schizophrenia", *Brain*, vol. 130, no. 9, pp. 2375–2386, 2007, ISSN: 0006-8950.

[63] C. D. Good, I. S. Johnsrude, J. Ashburner, R. N. Henson, K. J. Friston, and R. S. Frackowiak, "A voxel-based morphometric study of ageing in 465 normal adult human brains", *NeuroImage*, vol. 14, no. 1, pp. 21–36, 2001, ISSN: 10538119.

[64] C. Beckmann and S. Smith, "Probabilistic independent component analysis for functional magnetic resonance imaging", *IEEE Transactions on Medical Imaging*, vol. 23, no. 2, pp. 137–152, 2004, ISSN: 0278-0062.

[65] L. Griffanti, G. Douaud, J. Bijsterbosch, S. Evangelisti, F. Alfaro-Almagro, M. F. Glasser, E. P. Duff, S. Fitzgibbon, R. Westphal, D. Carone, C. F. Beckmann, and S. M. Smith, "Hand classification of fmri ica noise components", *NeuroImage*, vol. 154, pp. 188–205, 2017, ISSN: 1053-8119.

[66] L. D. Nickerson, S. M. Smith, D. Öngür, and C. F. Beckmann, "Using dual regression to investigate network shape and amplitude in functional connectivity analyses.", *Frontiers in neuroscience*, vol. 11, p. 115, 2017, ISSN: 1662-4548.

[67] C. Prévost, M. Pessiglione, E. Météreau, M.-L. Cléry-Melin, and J.-C. Dreher, "Separate valuation subsystems for delay and effort decision costs.", *The Journal of neuroscience : The official journal of the Society for Neuroscience*, vol. 30, no. 42, pp. 14 080–90, 2010, ISSN: 1529-2401.

[68] T. T.-J. Chong, M. Apps, K. Giehl, A. Sillence, L. L. Grima, and M. Husain, "Neurocomputational mechanisms underlying subjective valuation of effort costs", *PLOS Biology*, vol. 15, no. 2, B. Seymour, Ed., e1002598, 2017, ISSN: 1545-7885.

[69] J. S. Damoiseaux, S. A. R. B. Rombouts, F Barkhof, P Scheltens, C. J. Stam, S. M. Smith, and C. F. Beckmann, "Consistent resting-state networks across healthy subjects.", *Proceedings of the National Academy of Sciences of the United States of America*, vol. 103, no. 37, pp. 13 848–53, 2006, ISSN: 0027-8424.

A Appendix: LEiDA: full results

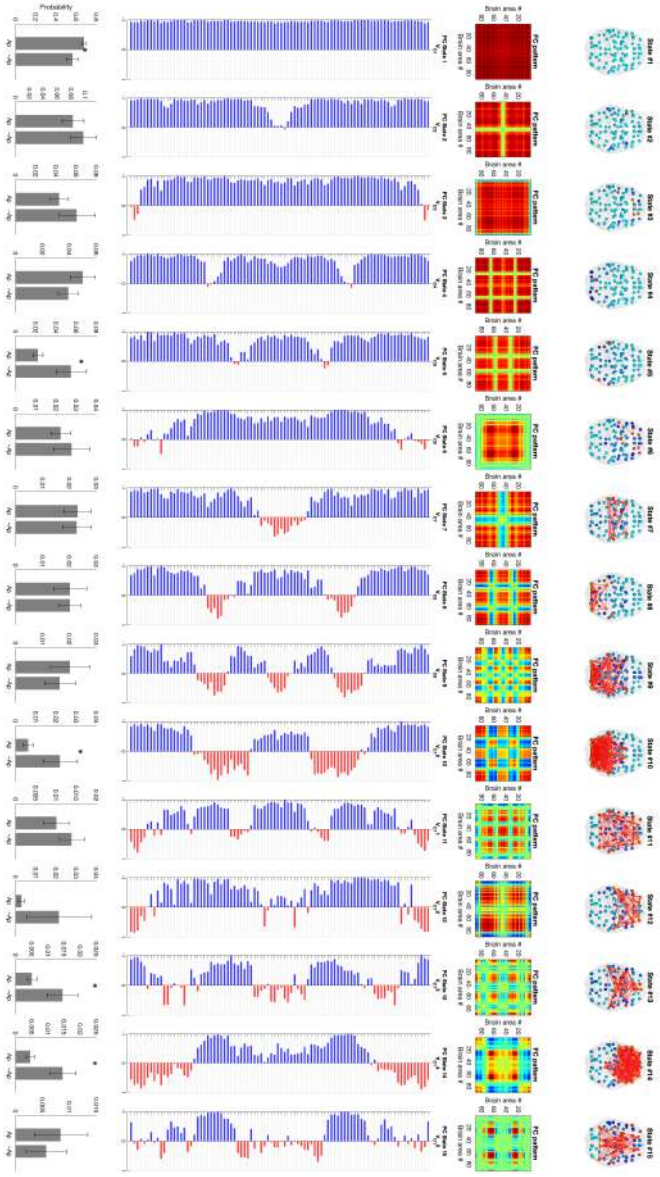

FIGURE A.1: Full results of the LEiDA analysis of the CADASIL dataset.

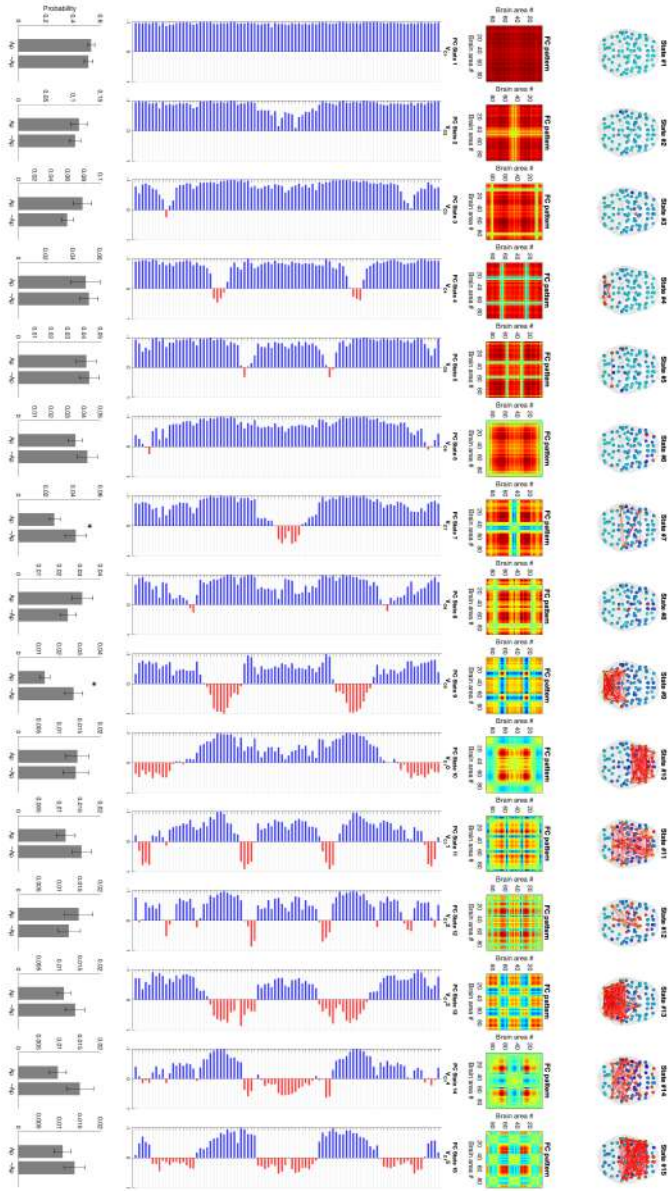

FIGURE A.2: Full results of the LEiDA analysis of the sporadic SVD dataset.

B Appendix: General analysis pipeline

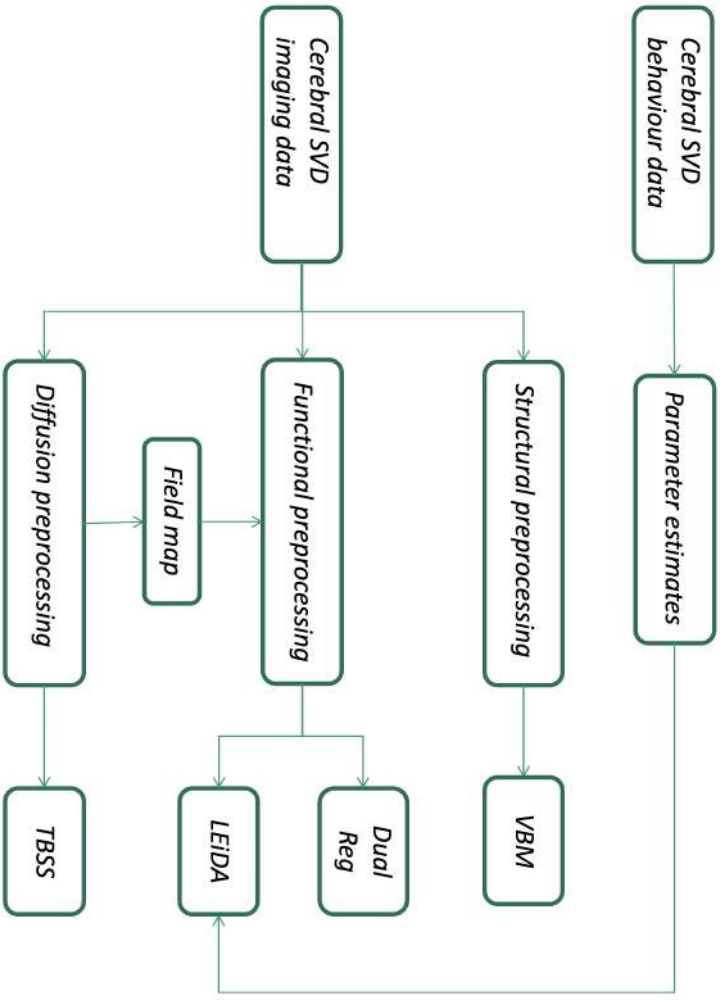

FIGURE B.1: Full pipeline of analysis used in this project.